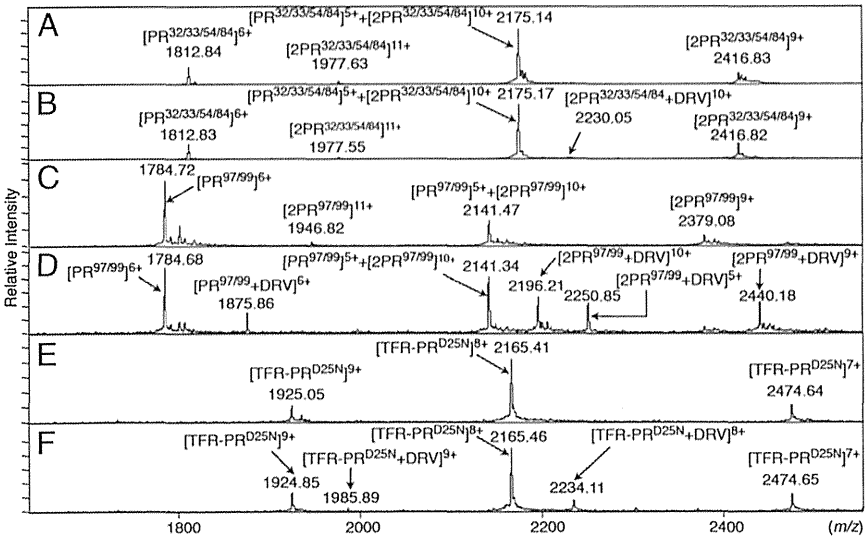

Fig. 3. ESI-MS spectra of $PR^{32/33/54/84}$, $PR^{97/99}$, and TFR-PR^{D25N}. (*A*) The ESI-MS spectrum of $PR^{32/33/54/84}$ (53.4 μM) without DRV. (*B*) The ESI-MS spectrum of $PR^{32/33/54/84}$ (55.6 μM) with DRV (400 μM). The addition of DRV showed only a small amount of DRV-bound $PR^{32/33/54/84}$ dimer ions, $[2PR^{32/33/54/84}+DRV]^{10+}$. (*C*) The ESI-MS spectrum of $PR^{97/99}$ (40.8 μM) in the absence of DRV. (*D*) The ESI-MS spectrum of $PR^{97/99}$ (40.3 μM) in the presence of DRV (120 μM). DRV binding to $PR^{97/99}$ yielded four additional peaks derived from $[PR^{97/99}+DRV]^{6+}$, $[2PR^{97/99}+DRV]^{10+}$, $[PR^{97/99}+DRV]^{5+}$, and $[2PR^{97/99}+DRV]^{9+}$. (*E*) The ESI-MS spectrum of TFR-PR^{D25N} (4.5 μM) without DRV. (*F*) The ESI-MS spectrum of TFR-PR^{D25N} (5.2 μM) with DRV (120 μM). Addition of DRV yielded two DRV-bound TFR-PR^{D25N} monomer ions, $[TFR\text{-}PR^{D25N}+DRV]^{9+}$ and $[TFR\text{-}PR^{D25N}+DRV]^{8+}$. The average masses of $PR^{32/33/54/84}$, $PR^{97/99}$, and TFR-PR^{D25N} are 10,870.92, 10,701.67, and 17,183.74, respectively.

differential scanning fluorimetry (DSF) (20). As illustrated in Fig. 5, the order of thermal stability was $PR^{WT} > PR^{D25N} > PR^{D29N} > PR^{32/33/54/84} > PR^{97/99} \sim PR^{T26A} > PR^{R87K} > PR^{1\text{-}C95A}$ (T_m; 53.37 > 52.18 > 51.02 > 50.17 > 48.22 ~ 48.12 > 47.02 > 44.46 °C, respectively). The difference in T_m values (ΔT_m) between PR^{D25N} and PR^{D29N} (1.16 °C) was less than ΔT_m between PR^{D25N} and $PR^{1\text{-}C95A}$ (7.72 °C), indicating that in terms of thermal stability, PR^{D25N} is closer to PR^{D29N} compared with the most unstable $PR^{1\text{-}C95A}$. Thus, PR^{D29N} monomer subunits are likely to interact at the active site interface and subsequently, at the termini interface, forming stable dimers. The DSF data, however, showed that T_m value of $PR^{97/99}$ (48.22 °C) was quite low compared with that of PR^{WT} (53.37 °C) and PR^{D29N} (51.02 °C), suggesting that $PR^{97/99}$ dimers are likely to be unstable. The T_m value of $PR^{1\text{-}C95A}$ was further lower (44.46 °C), suggesting that $PR^{1\text{-}C95A}$ dimers are also likely to be unstable (Fig. 5 *A* and *B*). Taking the ESI-MS and DSF results together, one can presume that the present ESI-MS assay detects both unstable (transient) and stable dimers. Furthermore, the present DSF data indicate that the stability of $PR^{97/99}$ and $PR^{1\text{-}C95A}$ dimers was lower than that of PR^{D25N} dimer (dimer dissociation constant; $K_D = 1.3$ μM), suggesting that the K_D values of transient dimers were higher than 1.3 μM (21). Thus, the present DSF data corroborate the above ESI-MS data showing that the HIV-1 PR dimerization process undergoes two steps (Fig. 4).

We previously reported that DRV inhibits not only proteolytic activity but also PR dimerization, whereas two FDA-approved anti-HIV-1 drugs, saquinavir (SQV) and nelfinavir (NFV), have no dimerization inhibition activity as examined with the FRET-based HIV-1 expression system (Fig. S1*A*) (13). To analyze the mechanism of the PR dimerization inhibition by DRV, we therefore examined the binding properties of DRV, SQV, and NFV with PR^{WT} (Fig. 6 *A–D*). The ESI-MS spectrum of PR^{WT} without drugs showed four peaks derived from differently charged ions, $[PR^{WT}]^{6+}$, $[2PR^{WT}]^{11+}$, $[PR^{WT}]^{5+}+[2PR^{WT}]^{10+}$, and $[2PR^{WT}]^{9+}$ (Fig. 6*A*). In the presence of DRV, four additional peaks appeared, ($[PR^{WT}+DRV]^{6+}$, $[2PR^{WT}+DRV]^{10+}$, $[PR^{WT}+DRV]^{5+}$, and $[2PR^{WT}+DRV]^{9+}$) (Fig. 6*B*). Additional analysis of the isotopologue ion peaks with PR^{D25N} in the presence of DRV confirmed the identity of monomer and dimer ions, as shown in Fig. S3 *F–I* and Table S2.

On the other hand, the binding of SQV to PR^{WT} yielded only two additional peaks, $[2PR^{WT}+SQV]^{10+}$ and $[2PR^{WT}+SQV]^{9+}$ (Fig. 6*C*), indicating that SQV binds only to PR^{WT} dimers, not to monomers. In the presence of NFV, as in the case of SQV, two additional peaks, $[2PR^{WT}+NFV]^{10+}$ and $[2PR^{WT}+NFV]^{9+}$, were identified (Fig. 6*D*). The relatively weak intensity of SQV- and NFV-bound PR^{WT} dimers is presumably due to their relatively low binding affinity to PR^{WT}, as previously demonstrated by Dierynk et al. (22). Taken together, these data indicate that SQV and NFV bind to PR^{WT} dimers but not to monomers, and DRV inhibits PR dimerization by binding to PR monomers in a one-to-one molar ratio.

Highly DRV-resistant HIV-1 isolates we previously generated in vitro (14) had acquired a unique combination of four amino acid substitutions (V32I/L33F/I54M/I84V), and DRV had decreased its binding to PR monomers containing such four amino acid substitutions (Fig. S1*B*) (14, 15). We therefore examined whether such four amino acid substitutions altered the binding profiles of DRV with PR, using ESI-MS. The ESI-MS spectrum of $PR^{32/33/54/84}$ refolded in the absence of DRV showed four

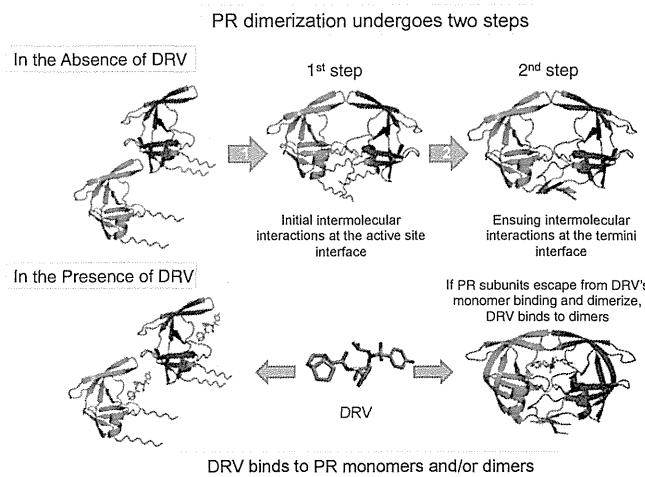

Fig. 4. The HIV-1 PR dimerization process undergoes two steps, and DRV inhibits the first step of PR dimerization by binding to PR monomers. PR subunits initially interact at the active site interface, generating unstably dimerized PR subunits, and subsequently the termini interface interactions occur, completing the dimerization process, generating stable PR dimers. DRV binds in the proximity of the active site interface of PR and blocks PR subunits dimerization. If PR subunits escape from the DRV's monomer binding and dimerize, DRV binds to PR dimers.

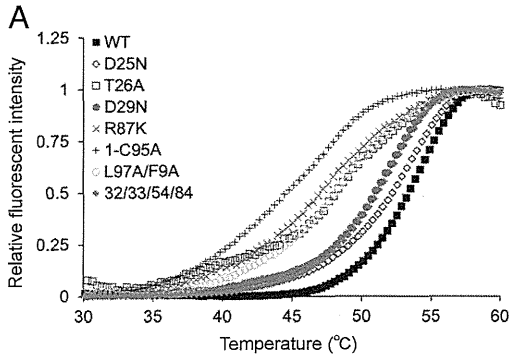

B

mutants	Tm (°C)
PR^{WT}	53.37±0.22
PR^{D25N}	52.18±0.24
PR^{T26A}	48.12±0.61
PR^{D29N}	51.02±0.22
$PR^{97/99}$	48.22±0.57
$PR^{1\text{-}C95A}$	44.46±0.69
$PR^{32/33/54/84}$	50.17±0.07

Fig. 5. Thermal stability of PR^{WT} and various mutated PR species determined using DSF. (*A*) Thermal denaturation, which was detected using SYPRO Orange, of PR^{WT}, PR^{D25N}, PR^{T26A}, PR^{D29N}, PR^{R87K}, $PR^{1\text{-}C95A}$, $PR^{L97A/F9A}$, and $PR^{32/33/54/84}$. (*B*) T_m values (the temperature at which the relative fluorescent intensity is 0.5) of each PR species.

peaks derived from five differently charged ions, $[PR^{32/33/54/84}]^{6+}$, $[2PR^{32/33/54/84}]^{11+}$, $[PR^{32/33/54/84}]^{5+}$+$[2PR^{32/33/54/84}]^{10+}$, and $[2PR^{32/33/54/84}]^{9+}$ (Fig. 3*A*). However, in the presence of DRV, only a substantially low peak representing DRV-bound $PR^{32/33/54/84}$ dimers, $[2PR^{32/33/54/84}+DRV]^{10+}$, was detected at *m/z* 2,230.05, and no DRV-bound PR monomers were detected (Fig. 3*B*). Thus, it seems that the loss of binding affinity to $PR^{32/33/54/84}$ in the monomeric form is greater than that in the dimeric form. Furthermore, we determined whether DRV binds to a mutated PR containing two substitutions (L97A/F99A; $PR^{97/99}$), which play important roles for the termini interface interactions but have no association with DRV resistance. The ESI-MS spectrum of $PR^{97/99}$ without DRV showed four peaks, $[PR^{97/99}]^{6+}$, $[2PR^{97/99}]^{11+}$, $[PR^{97/99}]^{5+}$+$[2PR^{97/99}]^{10+}$, and $[2PR^{97/99}]^{9+}$ (Fig. 3*C*). However, in the presence of DRV, four additional peaks appeared, $[PR^{97/99}+DRV]^{6+}$, $[2PR^{97/99}+DRV]^{10+}$, $[PR^{97/99}+DRV]^{5+}$, and $[2PR^{97/99}+DRV]^{9+}$ (Fig. 3*D*). Thus, L97 and F99 are not critical for DRV's monomer binding. The present data showed that the current ESI-MS method we used in this study is useful in detecting DRV's specific binding to PR^{WT}.

Finally, we asked whether DRV had an ability to bind to the PR precursor protein, Gag-Pol polyprotein, which is produced through the frame-shifting process in the Gag-encoding gene translation (Fig. S5 *A* and *B*) and subsequently maturates after the due excision through autoproteolysis (23–26). To examine the DRV binding to the PR precursor protein, a transframe precursor form of PR containing D25N substitution, TFR-PR^{D25N}, was constructed (Fig. S5*C*). In the absence of drugs, TFR-PR^{D25N} generated $[TFR\text{-}PR^{D25N}]^{10+}$, $[TFR\text{-}PR^{D25N}]^{9+}$, $[TFR\text{-}PR^{D25N}]^{8+}$, and $[TFR\text{-}PR^{D25N}]^{7+}$ (Fig. 3*E*), indicating that TFR-PR^{D25N} failed to dimerize, in line with the NMR data reported by Ishima et al. (19). In the presence of DRV two additional peaks, $[TFR\text{-}PR^{D25N}+DRV]^{8+}$ and $[TFR\text{-}PR^{D25N}+DRV]^{9+}$, appeared (Fig. 3*F*), indicating that DRV bound to TFR-PR^{D25N} monomers. In this regard, Agniswarmy et al. (27) have shown that the addition of C terminus four amino acids (PISP) to TFR-PR increases thermal stability of DRV-bound TFR-PR. In the present study we generated TFR-$PR^{D25N\text{-}7AA}$, which contained an additional seven N terminus amino acids of reverse transcriptase (7AA; PISPIET) at the C terminus of TFR-PR^{D25N}. The ESI-MS revealed that TFR-$PR^{D25N\text{-}7AA}$ formed dimers (Fig. S6*A*), suggesting that the addition of the seven amino acids allowed TFR-$PR^{D25N\text{-}7AA}$ to dimerize, probably by giving TFR-$PR^{D25N\text{-}7AA}$ proper conformation. The ESI-MS then showed that DRV binds to both TFR-$PR^{D25N\text{-}7AA}$ monomers and dimers (Fig. S6*B*). These results strongly suggest that the loss of dimerization ability of TFR-PR^{D25N} resulted in the loss of DRV's dimer binding.

Discussion

In the present study we constructed three "active site interface PR mutants" (PR^{T26A}, PR^{D29N}, and PR^{R87K}) and two "termini interface PR mutants" ($PR^{1\text{-}C95A}$ and $PR^{97/99}$) and determined their ESI-MS profiles. In the ESI-MS spectra, the peaks of PR^{D29N} monomers ($[PR^{D29N}]^{6+}$ and $[PR^{D29N}]^{7+}$) were greater than those of PR^{WT} ($[PR^{WT}]^{6+}$ and $[PR^{WT}]^{7+}$) (Fig. 2 *A* and *C*). The peaks of PR^{D29N} monomers ($[PR^{D29N}]^{6+}$ and $[PR^{D29N}]^{7+}$) were also greater than those of PR^{D29N} dimers ($[2PR^{D29N}]^{9+}$ and $[2PR^{D29N}]^{11+}$) (Fig. 2*C*). The same was true for the cases of $PR^{1\text{-}C95A}$ and $PR^{97/99}$ (Figs. 2*F* and 3*C*). These findings suggest that the dimers represent small components in the three mutated PR species. However, as assessed using the FRET-based HIV-1 expression assay, PR^{D29N} dimerization was apparently completely disrupted (13). Of particular note, the FRET-based system determines the FRET signal (CFP fluorescence after photobleaching/CFP fluorescence before photobleaching: $CFP^{A/B}$ ratio) in one cell at one time, accumulates ~20–30 cells' data, and obtains the average of the $CFP^{A/B}$ ratios. Then, if the average value is greater than 1.0, it is judged that FRET occurred, indicating that PR dimerization took place within the cell. However, there is variability in the $CFP^{A/B}$ ratios within the assay data, probably due to, but not limited to (*i*) unequal expression of PR proteins; (*ii*) uneven occurrence of protein–protein interactions (i.e., dimerization); and (*iii*) differing compartmentalization of the expressed PR species within the transfected cell population. Nevertheless, the FRET-based HIV-1 expression assay system only calls whether FRET occurred or did not occur. Thus, the FRET-based HIV-1 expression assay system inherently fails to identify the presence of a small amount of dimers or monomers. Therefore, in the case of PR^{D29N}, the FRET signal was determined as "not detected" (13). However, the ESI-MS system we used in the present study directly and more quantitatively identifies PR monomers and dimers. Thus, the ESI-MS system correctly recognized both a major fraction of PR^{D29N} monomers as well as a minor fraction of PR^{D29N} dimers. Accordingly, increasing the expression of PR^{D29N} by increasing the amount of plasmid for transfection does not increase the specific FRET-based signal, which we have confirmed in our initial conditioning phase of the construction of the system. Both PR^{T26A} and PR^{R87K} failed to dimerize as examined with the FRET-based HIV-1 expression assay, and no dimerized PR species were seen in the ESI-MS spectra (Fig. S4 and Table S1). When we examined the ESI-MS spectra of $PR^{1\text{-}C95A}$ and $PR^{97/99}$, the peaks of +6 charged monomer ions were much greater than in the PR^{WT} spectrum; however, PR dimer species were also present (Figs. 2*F* and 3*C*). Moreover, DSF analysis showed that $PR^{1\text{-}C95A}$ and $PR^{97/99}$ dimers were unstable (Fig. 5). Taking these data together, it is strongly suggested that the PR dimerization process undergoes two steps: (*i*) initial albeit weak intermolecular interactions occurring in the active site interface, and (*ii*) subsequent interactions

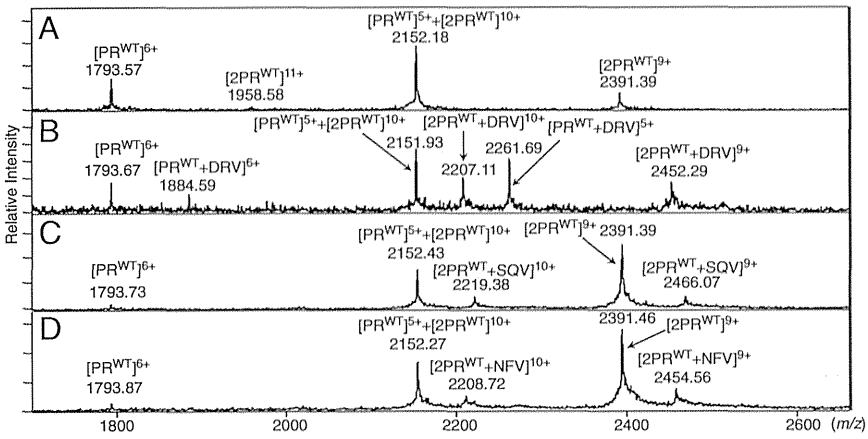

Fig. 6. The binding properties of DRV, SQV, and NFV to wild-type PR. (*A*) ESI-MS spectra of PR^{WT} (10.0 μM) in the absence of DRV, obtained by Bio-Tof-Q. (*B–D*) ESI-MS spectra of PR^{WT} in the presence of DRV, SQV, and NFV (all 120 μM); the final concentrations of PR^{WT} were 10.0, 9.5, and 14.4 μM, respectively. (*B*) Addition of DRV yielded four DRV-bound PR^{WT} ions, $[PR^{WT}+DRV]^{6+}$, $[2PR^{WT}+DRV]^{10+}$, $[PR^{WT}+DRV]^{5+}$, and $[2PR^{WT}+DRV]^{9+}$. (*C*) In the presence of SQV, two SQV-bound PR^{WT} dimer ions, $[2PR^{WT}+SQV]^{10+}$ and $[2PR^{WT}+SQV]^{9+}$, were observed, whereas SQV-bound PR^{WT} monomer ion were not seen. (*D*) Addition of NFV yielded two NFV-bound PR^{WT} dimer ions, $[2PR^{WT}+NFV]^{10+}$ and $[2PR^{WT}+NFV]^{9+}$, whereas no NFV-bound PR^{WT} monomer ions were present. The average mass of DRV, SQV, and NFV are 547.66, 670.85, and 567.31, respectively.

occurring in the termini interface, resulting in the complete and tight PR dimerization (Fig. 4).

In the present study, we also demonstrated that DRV binds to PR^{WT} monomers as well as dimers, whereas other "conventional" PIs, including SQV and NFV, bind only to dimers (Fig. 6 *A–D*), confirming that DRV uniquely has dual activity against PR^{WT}: inhibition of PR^{WT} dimerization and proteolytic activity as previously described (13). It is also noteworthy that the present data clearly showed that DRV binds to PR^{WT} monomer subunit in a one-to-one molar ratio.

We have previously selected highly DRV-resistant HIV-1 variants ($HIV_{DRV}{}^{R}$) and identified that $HIV_{DRV}{}^{R}$ had acquired a unique combination of four amino acid substitutions (V32I/L33F/I54M/I84V) in the proximity of the active site interface of its PR (Fig. 1) (14). In the present data DRV virtually completely failed to bind to $PR^{32/33/54/84}$ monomers, and only a small amount of DRV-bound $PR^{32/33/54/84}$ dimers was identified (Fig. 3*B*). However, L97A and F99A substitutions did not affect DRV's monomer and dimer binding (Fig. 3*D*). These results indicate that the binding domain in PR monomers for DRV is located distantly from the termini interface and is close to the active site interface, in line with the results of computational results reported by Huang et al. (28). Thus, the present ESI-MS analysis results strongly suggest that DRV blocks the first step of the PR dimerization process involving the active site interface, by binding to PR monomers in a one-to-one molar ratio (Fig. 4).

We have shown that once stable PR^{WT} dimers are formed, DRV no longer disrupts the dimers, as examined using the FRET-based assay (13). To ask whether DRV's binding to PR^{WT} monomers yields sufficient force to block PR^{WT} dimerization, the determination of the binding affinity of DRV for the folded monomers seems to be technically highly challenging. However, the present ESI-MS data showed that the amount of DRV-bound PR^{WT} monomers seemed to be greater than that of DRV-bound PR^{WT} dimers (Fig. 6*B*). Moreover, we determined the thermal stability of DRV-bound PR^{WT}, which apparently contains more DRV-bound PR^{WT} monomers than DRV-bound PR^{WT} dimers (Fig. 6*B*). As illustrated in Fig. S7, PR^{WT} was found to be highly stable as examined using the differential scanning fluorimetry (DSF), strongly suggesting that DRV fairly strongly binds to PR^{WT} monomer. The DSF data also suggested that DRV's binding to PR^{WT} monomers should have sufficient force to block PR^{WT} dimerization, inhibiting the formation of transient dimers. It is of note that if the formation of transient dimers (first step of the dimerization process) is blocked by DRV, the formation of stable dimers through the termini interface interactions (second step of the dimerization step) no longer occurs (Fig. 4). The determination of the exact binding site of PR monomer for DRV awaits further investigation, such as crystallographic analysis of PR monomer complexed with DRV and other dimerization inhibitors (13, 29, 30).

Louis et al. (24) have recently demonstrated that among nine FDA-approved PIs, DRV and SQV most potently block the autoproteolytic processing of the precursor construct (TFR-PR). Davis et al. (26) also demonstrated that among six FDA-approved HIV-1 PIs, DRV and SQV most potently block the initial step of autoproteolytic processing of Gag-Pol polyprotein by embedded dimerized PR. These data strongly suggest that DRV and SQV bind to TFR-PR, although the dynamics of the DRV binding remain elusive (26). In the present work DRV bound to TFR-$PR^{D25N-7AA}$ monomers and dimers (Fig. S6 *A* and *B*), in line with the data by Louis et al. (24), and our data strongly suggest that DRV blocks the autoproteolytic processing of Gag-Pol polyproteins through binding to the PR precursors (monomers and dimers) within the Gag-Pol polyprotein, contributing to DRV's potent antiretroviral activity against HIV-1. As for SQV, which has a greater K_D value (1.2×10^{-9} M) for binding to PR^{WT} than DRV (4.1×10^{-13} M) (22), Sayer and Louis (31) have shown that D25N substitution substantially decreases SQV's binding affinity to PR. Indeed, the present ESI-MS data also showed that SQV fails to bind to PR^{D25N}, TFR-PR^{D25N}, and TFR-$PR^{D25N-7AA}$ (Fig. S6*C* and S8 *A–C*). Thus the levels of SQV binding to these PR mutants carrying D25N substitution do not seem to be sufficient to be detected by ESI-MS.

A few groups have reported PR dimerization inhibitors targeting the terminal interface of PR (9–12). However, none of such inhibitors have been of clinical utility, probably because PR dimers, once formed, are highly stable to "de-dimerize" with the potent dimerization forces in the termini interface (13). On the other hand, the active site interface interactions play a critical role for PR dimerization, but the dimers formed are thought to be relatively unstable. Thus the development of new dimerization inhibitors targeting the active site interface would be highly suitable. It is also noteworthy that the ESI-MS approach is more quantitative than the FRET-based HIV-1 expression system, and we demonstrated two features: (*i*) DRV binds to PR^{WT} monomers and dimers, whereas (*ii*) DRV binds only to TFR-PR^{D25N} monomers. Thus, ESI-MS analysis is useful in analyzing how PR monomers and dimers act in the presence or absence of dimerization-targeting drugs. The new findings demonstrated in the present study should help understand the mechanism of HIV-1 PR inhibition and should also help develop novel and more potent PIs.

Materials and Methods

Vector Construction. The expression vectors containing the HIV-1 PR gene (pET-TFR-PR_{NL4-3}, pET-PR_{NL4-3}, and pET-$PR^{1\text{-}C95A}$) were constructed by using the In-Fusion HD Cloning Kit (Clontech). The other mutants (PR^{WT}, PR^{D25N},

PR^{T26A}, PR^{D29N}, PR^{R87K}, $PR^{32/33/54/84}$, and TFR-PR^{D25N}) were generated using the PrimeSTAR mutagenesis protocol (TaKaRa). More details are described in *SI Materials and Methods*.

FRET Procedure. The generation of the FRET-based HIV-1 expression system using CFP- and YFP-tagged HIV-1 PR-encoding plasmids we previously reported (13) is described in *SI Materials and Methods*.

Protein Preparation. The protein expression using plasmids we generated was induced by addition of 1 mM isopropyl β-D-thiogalactopyranoside. PR was purified by using buffer A (20 mM Tris, 1 mM EDTA, and 1 mM DTT), and buffer A containing 2 M Urea was used. The expressed PR was solubilized with 50 mM formic acids (pH 2.8). The unfolded PR refolded with a neutralizing buffer [100 mM ammonium acetate, pH 6.0, 2% (vol/vol) methanol]. More details are described in *SI Materials and Methods*.

Thermal Stability Analysis Using DSF. In the DSF analysis, the final concentration of refolded PR mutants was 7–10 μM. SYPRO Orange (Life Technologies) was then added to the PR solution (final concentration of SYPRO orange: 5×) (20). Thirty microliters of the PR solution was successively heated from 25 °C to 95 °C, and changes of the fluorescence intensity were documented by the real-time PCR system 7500 Fast (Applied Biosystems). More details are described in *SI Materials and Methods*.

Analysis with ESI-MS. MS spectra of PR^{D25N} with and without DRV were obtained using a Bio-Tof-Q ESI quadrupole time-of-flight mass spectrometer (Bruker Daltonics). For the isotopologue ion peak analysis, high-resolution mass spectrometry was performed on a Bruker SolariX 9.4T FT-ICR MS (for PR^{D25N}) or a Bruker SolariX 7T FT-ICR MS (for PR^{T26A} and PR^{R87K}). More details are described in *SI Materials and Methods*.

ACKNOWLEDGMENTS. This work was supported in part by a grant for the Global Education and Research Center Aiming at the Control of AIDS (Global Center of Excellence, supported by Monbu-Kagakusho); Promotion of AIDS Research from the Ministry of Health, Welfare, and Labor of Japan; a grant to the Cooperative Research Project on Clinical and Epidemiological Studies of Emerging and Reemerging Infectious Diseases (Renkei Jigyo, no. 78; Kumamoto University) of Monbu-Kagakusho (to H.M.); the Intramural Research Program of the Center for Cancer Research, National Cancer Institute, National Institutes of Health (H.M.); and by Extramural Grant GM53386 from the National Institutes of Health (to A.K.G.).

1. Wlodawer A, et al. (1989) Conserved folding in retroviral proteases: Crystal structure of a synthetic HIV-1 protease. *Science* 245(4918):616–621.
2. Babé LM, Rosé J, Craik CS (1995) Trans-dominant inhibitory human immunodeficiency virus type 1 protease monomers prevent protease activation and virion maturation. *Proc Natl Acad Sci USA* 92(22):10069–10073.
3. Weber IT (1990) Comparison of the crystal structures and intersubunit interactions of human immunodeficiency and Rous sarcoma virus proteases. *J Biol Chem* 265(18): 10492–10496.
4. Strisovsky K, Tessmer U, Langner J, Konvalinka J, Kräusslich HG (2000) Systematic mutational analysis of the active-site threonine of HIV-1 proteinase: Rethinking the "fireman's grip" hypothesis. *Protein Sci* 9(9):1631–1641.
5. Todd MJ, Semo N, Freire E (1998) The structural stability of the HIV-1 protease. *J Mol Biol* 283(2):475–488.
6. Ishima R, Torchia DA, Louis JM (2007) Mutational and structural studies aimed at characterizing the monomer of HIV-1 protease and its precursor. *J Biol Chem* 282(23): 17190–17199.
7. Louis JM, et al. (2003) Revisiting monomeric HIV-1 protease. Characterization and redesign for improved properties. *J Biol Chem* 278(8):6085–6092.
8. Louis JM, Ishima R, Torchia DA, Weber IT (2007) HIV-1 protease: Structure, dynamics, and inhibition. *Adv Pharmacol* 55:261–298.
9. Babé LM, Rosé J, Craik CS (1992) Synthetic "interface" peptides alter dimeric assembly of the HIV 1 and 2 proteases. *Protein Sci* 1(10):1244–1253.
10. Shultz MD, et al. (2004) Small-molecule dimerization inhibitors of wild-type and mutant HIV protease: A focused library approach. *J Am Chem Soc* 126(32):9886–9887.
11. Shultz MD, Chmielewski J (1999) Probing the role of interfacial residues in a dimerization inhibitor of HIV-1 protease. *Bioorg Med Chem Lett* 9(16):2431–2436.
12. Davis DA, et al. (2006) Inhibition of HIV-1 replication by a peptide dimerization inhibitor of HIV-1 protease. *Antiviral Res* 72(2):89–99.
13. Koh Y, et al. (2007) Potent inhibition of HIV-1 replication by novel non-peptidyl small molecule inhibitors of protease dimerization. *J Biol Chem* 282(39):28709–28720.
14. Koh Y, et al. (2010) In vitro selection of highly darunavir-resistant and replication-competent HIV-1 variants by using a mixture of clinical HIV-1 isolates resistant to multiple conventional protease inhibitors. *J Virol* 84(22):11961–11969.
15. Koh Y, et al. (2011) Loss of protease dimerization inhibition activity of darunavir is associated with the acquisition of resistance to darunavir by HIV-1. *J Virol* 85(19): 10079–10089.
16. Loo JA (2000) Electrospray ionization mass spectrometry: A technology for studying noncovalent macromolecular complexes. *Int J Mass Spectrom* 200(1-3):175–186.
17. Loo JA, et al. (1998) Application of electrospray ionization mass spectrometry for studying human immunodeficiency virus protein complexes. *Proteins* 33(Suppl 2): 28–37.
18. Senko MW, Beu SC, McLaffertycor FW (1995) Determination of monoisotopic masses and ion populations for large biomolecules from resolved isotopic distributions. *J Am Soc Mass Spectrom* 6(4):229–233.
19. Ishima R, Torchia DA, Lynch SM, Gronenborn AM, Louis JM (2003) Solution structure of the mature HIV-1 protease monomer: Insight into the tertiary fold and stability of a precursor. *J Biol Chem* 278(44):43311–43319.
20. Niesen FH, Berglund H, Vedadi M (2007) The use of differential scanning fluorimetry to detect ligand interactions that promote protein stability. *Nat Protoc* 2(9): 2212–2221.
21. Sayer JM, Liu F, Ishima R, Weber IT, Louis JM (2008) Effect of the active site D25N mutation on the structure, stability, and ligand binding of the mature HIV-1 protease. *J Biol Chem* 283(19):13459–13470.
22. Dierynck I, et al. (2007) Binding kinetics of darunavir to human immunodeficiency virus type 1 protease explain the potent antiviral activity and high genetic barrier. *J Virol* 81(24):13845–13851.
23. Sadiq SK, Noé F, De Fabritiis G (2012) Kinetic characterization of the critical step in HIV-1 protease maturation. *Proc Natl Acad Sci USA* 109(50):20449–20454.
24. Louis JM, Aniana A, Weber IT, Sayer JM (2011) Inhibition of autoprocessing of natural variants and multidrug resistant mutant precursors of HIV-1 protease by clinical inhibitors. *Proc Natl Acad Sci USA* 108(22):9072–9077.
25. Pettit SC, Everitt LE, Choudhury S, Dunn BM, Kaplan AH (2004) Initial cleavage of the human immunodeficiency virus type 1 GagPol precursor by its activated protease occurs by an intramolecular mechanism. *J Virol* 78(16):8477–8485.
26. Davis DA, et al. (2012) Activity of human immunodeficiency virus type 1 protease inhibitors against the initial autocleavage in Gag-Pol polyprotein processing. *Antimicrob Agents Chemother* 56(7):3620–3628.
27. Agniswamy J, Sayer JM, Weber IT, Louis JM (2012) Terminal interface conformations modulate dimer stability prior to amino terminal autoprocessing of HIV-1 protease. *Biochemistry* 51(5):1041–1050.
28. Huang D, Caflisch A (2012) How does darunavir prevent HIV-1 protease dimerization? *J Chem Theory Comput* 8(5):1786–1794.
29. Amano M, et al. (2013) GRL-0519, a novel oxatricyclic ligand-containing nonpeptidic HIV-1 protease inhibitor (PI), potently suppresses replication of a wide spectrum of multi-PI-resistant HIV-1 variants in vitro. *Antimicrob Agents Chemother* 57(5): 2036–2046.
30. Aoki M, et al. (2012) Loss of the protease dimerization inhibition activity of tipranavir (TPV) and its association with the acquisition of resistance to TPV by HIV-1. *J Virol* 86(24):13384–13396.
31. Sayer JM, Louis JM (2009) Interactions of different inhibitors with active-site aspartyl residues of HIV-1 protease and possible relevance to pepsin. *Proteins* 75(3):556–568.

Antiviral Research 106 (2014) 1–4

Contents lists available at ScienceDirect

Antiviral Research

journal homepage: www.elsevier.com/locate/antiviral

Short Communication

Probing the molecular mechanism of action of the HIV-1 reverse transcriptase inhibitor 4′-ethynyl-2-fluoro-2′-deoxyadenosine (EFdA) using pre-steady-state kinetics

Yagmur Muftuoglu [a,1], Christal D. Sohl [a,1], Andrea C. Mislak [a], Hiroaki Mitsuya [b,c,d], Stefan G. Sarafianos [e,f], Karen S. Anderson [a,*]

[a] Department of Pharmacology, Yale University School of Medicine, New Haven, CT 06520, United States
[b] Department of Infectious Diseases, Kumamoto University Graduate School of Medical Sciences, Kumamoto 860-8556, Japan
[c] Department of Hematology, Kumamoto University Graduate School of Medical Sciences, Kumamoto 860-8556, Japan
[d] Experimental Retrovirology Section, HIV and AIDS Malignancy Branch, National Cancer Institute, National Institutes of Health, Bethesda, MD 20892, United States
[e] CS Bond Life Sciences Center and Department of Molecular Microbiology and Immunology, University of Missouri, School of Medicine, Columbia, MO 65211, United States
[f] Department of Biochemistry, University of Missouri, School of Medicine, Columbia, MO 65211, United States

ARTICLE INFO

Article history:
Received 17 December 2013
Revised 2 March 2014
Accepted 3 March 2014
Available online 12 March 2014

Keywords:
HIV
Reverse transcriptase
Enzyme kinetics
EFdA
Polymerase

ABSTRACT

The novel antiretroviral 4′-ethynyl-2-fluoro-2′-deoxyadenosine (EFdA) is a potent nucleoside HIV-1 reverse transcriptase (RT) inhibitor (NRTI). Unlike other FDA-approved NRTIs, EFdA contains a 3′-hydroxyl. Pre-steady-state kinetics showed RT preferred incorporating EFdA-TP over native dATP. Moreover, RT slowly inserted nucleotides past an EFdA-terminated primer, resulting in delayed chain termination with unaffected fidelity. This is distinct from KP1212, another 3′-hydroxyl-containing RT inhibitor considered to promote viral lethal mutagenesis. New mechanistic features of RT inhibition by EFdA are revealed.

Nucleoside reverse transcriptase inhibitors (NRTIs) represent an important class of HIV-1 reverse transcriptase (RT) targeted therapy for treating HIV infection. All FDA-approved NRTIs lack a 3′-hydroxyl moiety that terminates DNA chain extension upon incorporation into the growing proviral DNA. Many NRTIs cause significant toxicity, often due to their interactions with the human mitochondrial DNA polymerase γ (pol γ) (Apostolova et al., 2011; Johnson et al., 2001; Nakata et al., 2007). A novel antiretroviral compound, 4′-ethynyl-2-fluoro-2′-deoxyadenosine (EFdA) (Fig. 1), has shown potency several orders of magnitude superior to the NRTIs currently prescribed against HIV-1 (Nakata et al., 2007) and low toxicity (Ohrui et al., 2007; Zhang et al., 2013). We have shown that EFdA is highly favored by RT (Michailidis et al., 2009), and incorporation by pol γ is nearly negligible (Sohl et al., 2012b), indicating a favorable compromise of RT potency and low pol γ-mediated toxicity. EFdA is currently under clinical development by Merck & Co. with Yamasa Corporation, Chiba, Japan.

Despite the promise of EFdA, characterization of the molecular mechanism of inhibition of RT has been limited to steady-state kinetic studies (Michailidis et al., 2009, 2013; Nakata et al., 2007), which report only on the rate-limiting step (in this case, product release). Here we use pre-steady-state kinetic analysis to determine critical kinetic parameters such as the maximum rate of analog incorporation, k_{pol}, the binding affinity of the incoming nucleotide or analog for the enzyme, K_d, and the efficiency of incorporation, k_{pol}/K_d, combined with extension, fidelity, and ATP and pyrophosphate (PPi)-mediated resistance studies to understand the mechanism of EFdA inhibition of RT.

Single-turnover conditions with enzyme in excess of primer/template substrate were used to determine the k_{pol} and K_d for single nucleotide or analog incorporation. A pre-incubated mixture of RT (purified as described previously) (Kerr and Anderson, 1997) and 5′-radiolabeled DNA primer/template substrate (Ray et al., 2002) were rapidly combined with excess magnesium chloride and varying concentrations of dATP or EFdA-TP (Fig. 1) using a RQF-3 rapid chemical quench (Kintek Instruments) for incubations

* Corresponding author. Address: Department of Pharmacology, Yale University School of Medicine, 333 Cedar St., New Haven, CT 06520, United States. Tel.: +1 203 785 4526; fax: +1 203 785 7670.
E-mail address: karen.anderson@yale.edu (K.S. Anderson).
[1] These authors contributed equally.

http://dx.doi.org/10.1016/j.antiviral.2014.03.001
0166-3542/

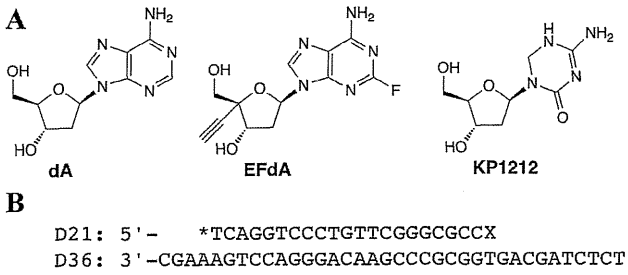

Fig. 1. Reagents used in the kinetic studies. (A) Chemical structures of dA and and the dA analog EFdA. An additional RT inhibitor containing a 3′-hydroxyl group, the dC analog KP1212, is also shown. (B) The D21/D36 primer/template substrate used in the incorporation and extension experiments. The asterisk indicates the radiolabel at the 5′ primer end, and the "X" denotes the site of incorporation of the incoming EFdA-TP or dATP. For the extension past EFdA and phosphorolytic studies, a pre-incorporated EFdAMP present at the primer "X" site (primer-EFdAMP/template substrate) is used.

ranging from 0.01 s to 3 s. Following reaction quenching with EDTA (0.34 M final), separation on a 20% polyacrylamide denaturing gel, and analysis via phosphorimaging (Bio-RAD Molecular Imager FX), plots of product formation versus time were generated and fit to single-exponential equations to determine the observed rates of polymerization (k_{obs}) for varying concentrations of dATP or EFdA-TP (KaleidaGraph). Hyperbolic fits of k_{obs} versus concentration plots yielded k_{pol} and K_d values (Table 1).

RT incorporated EFdA-TP over twofold more efficiently than dATP (Table 1). To date, only two other RT inhibitors are preferentially inserted over the native nucleotide by RT: 2′,3′-didehydro-3′-deoxythymidine (d4T) (Vaccaro et al., 2000) and 2′,3′-didehydro-3′-deoxy-4′-ethynylthymidine (Ed4T) (Sohl et al., 2012a). Based on findings of high potency (Nakata et al., 2007; Ohrui et al., 2007) and our results indicating efficient RT incorporation, we propose low doses of EFdA can be effective in HIV patients, minimizing toxicity (Nakata et al., 2007). Additionally, while RT is extremely poor at discriminating EFdA-TP from dATP (Table 1), discrimination by pol γ is over 9000-fold better than RT, indicating nearly negligible analog incorporation in the presence of native nucleotides. NMR studies suggest this difference in discrimination by pol γ relative to RT may come from the 4′-ethynyl and 3′-hydroxyl moieties of EFdA (Fig. 1A) which force the sugar into a Northern puckering conformation. This Northern conformation is preferred by RT for nucleotide insertion, while Southern puckering is favored by pol γ (Kirby et al., 2013, 2011). In summary, these discrimination findings support the high clinical potential of EFdA in that negligible incorporation by pol γ should lessen mitochondria-based toxicity.

EFdA is not the first proposed RT inhibitor to contain a 3′-hydroxyl group; a second RT inhibitor under development, KP1212 (Harris et al., 2005), also contains this moiety (Fig. 1A). In contrast to EFdA, RT incorporated KP1212 14-fold less efficiently than dCTP (Murakami et al., 2005). Human polymerase selectivity for KP1212 was poorer as well when compared to EFdA; pol γ incorporated KP1212 26-fold less efficiently than dCTP, which is less than a two-fold difference compared to RT discrimination (Murakami et al., 2005). Thus we propose the 4′-ethynyl group imparts more influence than the 3′-hydroxyl in contributing to the very high level discrimination by pol γ and highly efficient incorporation by RT.

In addition to changes in incorporation efficiencies, the antiviral inhibitors containing 3′-hydroxyl groups have other unique mechanisms of action. KP-1212 propagates error-prone G to A and A to G substitutions leading to lethal viral mutagenesis (Murakami et al., 2005; Mullins et al., 2011). Entecavir, a 2′-deoxyguanosine analog used for treating hepatitis B, also supports additional primer elongation by HIV RT and has been described as a delayed chain-terminating inhibitor (Domaoal et al., 2008; Tchesnokov et al., 2008). Thus we hypothesized EFdA may also support primer elongation. To probe this, RT or exonuclease-deficient pol γ (purified as described previously) (Sohl et al., 2012a) and the DNA primer-EFdAMP/template substrate (a primer containing a pre-incorporated EFdA monophosphate (Fig. 1B), prepared as described previously (Sohl et al., 2012a)) were incubated with a mixture of dATP, dCTP, TTP, and dGTP (30 μM each) and excess magnesium chloride. Both pol γ (Fig. 2A) and RT (Fig. 2B) completed full extension (past EFdA) of the primer-EFdAMP/template substrate. However, pol γ could only extend a small amount of the primer-EFdAMP/template substrate (12% of substrate converted to product) over the course of the assay, while RT extended 88%. Remarkably, after only 30 s, RT extended 51% of the primer-EFdAMP/template, and extension was essentially complete within 1 h (Fig. 2B). By quantifying the amount of fully extended product over time, an observed rate of complete template extension, k_{max}, of $0.0014 \pm 0.0002\ s^{-1}$ was measured for RT, while the small amount of product formed by pol γ generated a $k_{max} = 0.00024 \pm 0.00004\ s^{-1}$.

The rate of incorporation of a single correct nucleotide (dCTP) past EFdA in the primer-EFdAMP/template was measured for RT and pol γ (Table 2). The k_{pol} for RT was at least 30-fold higher than for pol γ; pol γ incorporated dCTP past EFdA so inefficiently that only an upper limit for k_{pol} could be reliably determined (Table 2). However, RT fully extended the primer in the presence of physiologically relevant concentrations of dNTPs in a timeframe of seconds to minutes, with a more distributive versus processive mechanism (as shown by laddering, Fig. 2B). This indicates that

Table 1
Pre-steady-state rate constants for incorporation of EFdA-TP or dATP by RT and pol γ.[a]

Enzyme	Nucleotide or analog	k_{pol} (s^{-1})	K_d (μM)	Efficiency[b] ($\mu M^{-1}\ s^{-1}$)	Discrimination[c]
RT	dATP	8.0 ± 0.7	3.8 ± 0.8	2.1	0.47
	EFdA-TP	5.8 ± 0.3	1.3 ± 0.2	4.5	
pol γ[d]	dATP	220 ± 16	3.2 ± 0.7	69	4,300
	EFdA-TP	0.29 ± 0.02	18 ± 4	0.016	

[a] Kinetic parameters determined from at least eight (RT), or at least seven (pol γ) single turnover experiments with varying dATP or EFdA-TP concentrations.
[b] Efficiency = k_{pol}/K_d.
[c] Discrimination = $\frac{efficiency dATP}{efficiency EFDA}$.
[d] Sohl et al. (2012b).

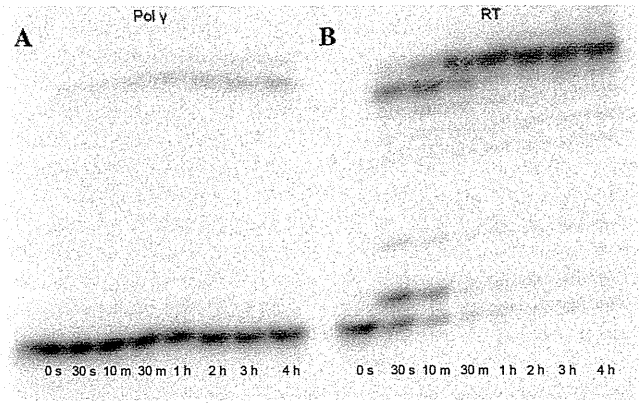

Fig. 2. Native nucleotide extension past pre-incorporated EFdA. (A) Extension by pol γ. The rate of formation of the final extended product, k_{max}, was $0.00024 \pm 0.00004\ s^{-1}$, with 12% of the substrate turned over to product. (B) Extension by RT. The value for k_{max} was $0.0014 \pm 0.0002\ s^{-1}$, with 88% of the substrate turned over to product. For both enzymes, the lanes represent 0 s, 30 s, 10 m, 30 m, 1 h, 2 h, 3 h, and 4 h. Experiments required 100 nM enzyme, 30 μM of each of the 4 dNTPs, and 25 nM of the primer-EFdAMP/template substrate.

Table 2
Pre-steady-state rate constants for post-EFdA incorporation of a single dCTP (the next correct nucleotide) by RT and pol γ.[a]

Enzyme	k_{pol} (s^{-1})	K_d (μM)	Efficiency[b] ($\mu M^{-1}\ s^{-1}$)
RT	0.0064 ± 0.0004	1.9 ± 0.4	0.0034[c]
pol γ	≤0.0002[d]	N.D.	N.D.

[a] Kinetic parameters determined from nine (RT) or seven (pol γ) single turnover experiments with varying dCTP concentrations.
[b] N.D.: not determined.
[c] Incorporation of dCTP after AMP in a similar primer/template has a measured efficiency of 1.5 $\mu M^{-1}\ s^{-1}$ (Kim et al., 2012).
[d] Incorporation of dCTP after AMP in a similar primer/template has a measured k_{pol} of 72 ± 3 s^{-1} (Sohl et al., 2013).

delayed chain termination is one mechanism of inhibition of RT by EFdA.

The efficiency of incorporation of nucleotides past EFdA by RT is lower than that seen with the delayed chain terminator entecavir. A 7-fold drop in efficiency is seen for the incorporation of the next correct nucleotide past entecavir (Tchesnokov et al., 2008) versus the over 1300-fold decrease for extension efficiency past EFdA by RT (Tables 1 and 2). As the k_{off} for DNA dissociation from RT is estimated to be 0.2 s^{-1} (Kellinger and Johnson, 2011), we expect that traditional chain termination, in addition to delayed chain termination, likely contributes to the overall mechanism of RT inhibition by EFdA. Our findings echo our previous work proposing chain termination via translocation inhibition that identified minor extension past EFdA at comparable time points (Michailidis et al., 2009). Given that nucleotide incorporation efficiency depends on the primer/template used (Iyidogan and Anderson, 2012), we used a biologically-relevant primer/template designed to mimic the polymerization binding site (PBS) for HIV RT. Our results describing delayed chain termination represent one important example of the effects EFdA can have on RT; additional mechanisms may be factors for effective RT inhibition as well.

Slowing extension past EFdA can affect RT using several mechanisms, including (1) extremely inefficient extension, which can promote stalling and dissociation resulting in a similar outcome as chain termination or (2) error-prone extension reminiscent of KP1212 (Murakami et al., 2005) promoting viral error catastrophe. Entecavir, while serving primarily as a delayed chain terminator, has also been shown to promote some error-prone extension (Domaoal et al., 2008). Efficiencies of incorporation (Table 2, *vide supra*) of dCTP, the next correct nucleotide past EFdA, decreased approximately 600-fold for RT, with a $\geqslant 10^6$-fold decrease in k_{pol} for pol γ when compared to the incorporation of dATP (Tables 1 and 2). In comparison, the incorporation efficiency for the next correct nucleotide after KP1212 decreased approximately 3.3-fold and 4.4-fold for RT and pol γ, respectively (Murakami et al., 2005). The nearly 200-fold difference in nucleotide incorporation efficiency by RT past KP1212 versus past EFdA indicates two unique inhibition mechanisms at work: while KP1212 functions by inducing mutagenesis, EFdA substantially slows DNA chain extension.

To determine if incorporation of EFdA alters the fidelity of chain extension, we assessed misincorporation of dATP or TTP (2 mM) opposite deoxyguanine in the primer-EFdAMP/template (25 nM) by RT (100 nM) in excess magnesium chloride. These misincorporation studies gave apparent k_{pol} (k_{pol_app}) values of $1.3 \times 10^{-3}\ s^{-1}$ for T:G and A:G by RT, which is 4- to 1000-fold slower than typical RT misincorporation rates (Feng and Anderson, 1999), and no product formation was observed for pol γ (same conditions, $k_{pol\_app} < 4.6 \times 10^{-5}\ s^{-1}$ for T:G and A:G). Overall efficiency for misincorporation by RT was extremely low due to weak binding of these nucleotide triphosphates. Thus we conclude that significantly slowing extension past EFdA is a primary mechanism of RT inhibition, rather than a loss of fidelity as seen with KP1212.

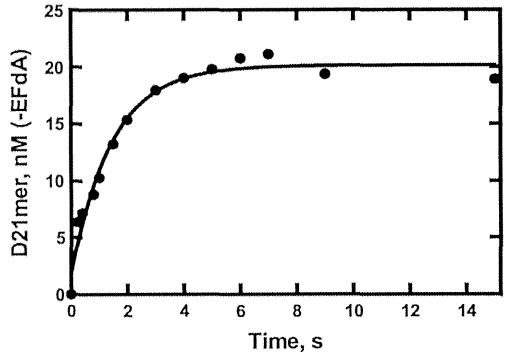

Fig. 3. PPi-based removal of an incorporated EFdA by RT. RT (250 nM) removes EFdA from the primer-EFdAMP/template (50 nM) in the presence of PPi (2 mM) using a rapid chemical quench. A rate of removal, $k_{removal}$, was calculated to be 0.69 ± 0.09 s^{-1}.

A mode of RT-mediated resistance to NRTIs is via phosphorolytic excision, in which RT uses either ATP or PPi to remove the incorporated inhibitor from the growing DNA strand. We probed the ability of RT (250 nM) to remove EFdA from the DNA primer-EFdAMP/template substrate (50 nM, Fig. 1B) in the presence either ATP (3 mM) or PPi (2 mM sodium pyrophosphate 10 hydrate) and excess magnesium chloride using a rapid chemical quench in conditions described previously (Ray et al., 2002). The removal by ATP-mediated pyrophosphorolysis was negligible, while removal with PPi was significant. We measured a rate of removal of EFdA, $k_{removal}$, of 0.69 ± 0.09 s^{-1} (Fig. 3). This is similar to the rate of PPi-based carbovir removal by RT (0.61 s^{-1}) (Ray et al., 2002). Interestingly, Tchesnokov et al. found that incorporating three nucleotides past entecavir by RT provided protection from ATP-mediated removal (Tchesnokov et al., 2008). While a $k_{removal}$ was not reported, entecavir removal was not complete even after 1 h (Tchesnokov et al., 2008), indicating a significantly slower rate than that seen for EFdA removal. Further, the rate of extension past entecavir by RT is similar to the rate of extension past EFdA (this rate is an estimate only, as a preincorporated entecavir primer/template was not used in this study, (Domaoal et al., 2008).) This indicates that extension past entecavir is likely to be highly favored over its removal, thereby inhibiting pyrophosphorolysis-based resistance. In contrast, the rate of incorporation of the next correct nucleotide past EFdA is over two orders of magnitude slower (Table 2) than the rate of its removal (Fig. 3). This indicates that EFdA removal is significantly favored over extension. We conclude that PPi-based removal of EFdA is a possible mode of resistance.

In summary, EFdA, a potent inhibitor of RT, functions at least in part by acting as a delayed chain terminator by slowing nucleotide extension after its highly efficient incorporation. These findings are similar to that seen with extension past entecavir by RT, although EFdA incorporation results in slower post-inhibitor incorporation efficiency and minimal changes in fidelity (Domaoal et al., 2008; Tchesnokov et al., 2008) relative to entecavir. Pyrophosphorolytic excision of EFdA by RT is a possible mode of resistance. The striking discrimination by pol γ in contrast with the preference of EFdA over dATP by RT indicates EFdA is a very promising RT inhibitor and sets an important benchmark for future NRTIs. Because of this discrimination profile, EFdA can likely be used in the clinical setting to treat HIV patients with lower doses and minimal mitochondrial-based toxicity. Understanding the mechanism of action employed by EFdA can help in the development and refinement of combination therapies for treating HIV, in addition to paving the way for the discovery of other HIV inhibitors with a similar mechanism.

Acknowledgments

This work was supported by NIH grants R01 GM049551 (to K.S.A.), F32 GM099289 (to C.D.S.), and AI076119, AI099284, AI100890, and GM103368 (to S.G.S.). We would like to thank Ligong Wang for the purification of the pol accessory subunit.

References

Apostolova, N., Blas-Garcia, A., Esplugues, J.V., 2011. Mitochondrial interference by anti-HIV drugs: mechanisms beyond Pol-gamma inhibition. Trends Pharmacol. Sci. 32, 715–725.

Domaoal, R.A., McMahon, M., Thio, C.L., Bailey, C.M., Tirado-Rives, J., Obikhod, A., Detorio, M., Rapp, K.L., Siliciano, R.F., Schinazi, R.F., Anderson, K.S., 2008. Pre-steady-state kinetic studies establish entecavir 5′-triphosphate as a substrate for HIV-1 reverse transcriptase. J. Biol. Chem. 283, 5452–5459.

Feng, J.Y., Anderson, K.S., 1999. Mechanistic studies comparing the incorporation of (+) and (−) isomers of 3TCTP by HIV-1 reverse transcriptase. Biochemistry 38, 55–63.

Harris, K.S., Brabant, W., Styrchak, S., Gall, A., Daifuku, R., 2005. KP-1212/1461, a nucleoside designed for the treatment of HIV by viral mutagenesis. Antiviral Res. 67, 1–9.

Iyidogan, P., Anderson, K.S., 2012. Understanding the molecular mechanism of sequence dependent tenofovir removal by HIV-1 reverse transcriptase: differences in primer binding site versus polypurine tract. Antiviral Res. 95, 93–103.

Johnson, A.A., Ray, A.S., Hanes, J., Suo, Z., Colacino, J.M., Anderson, K.S., Johnson, K.A., 2001. Toxicity of antiviral nucleoside analogs and the human mitochondrial DNA polymerase. J. Biol. Chem. 276, 40847–40857.

Kellinger, M.W., Johnson, K.A., 2011. Role of induced fit in limiting discrimination against AZT by HIV reverse transcriptase. Biochemistry 50, 5008–5015.

Kerr, S.G., Anderson, K.S., 1997. RNA dependent DNA replication fidelity of HIV-1 reverse transcriptase: evidence of discrimination between DNA and RNA substrates. Biochemistry 36, 14056–14063.

Kim, J., Roberts, A., Yuan, H., Xiong, Y., Anderson, K.S., 2012. Nucleocapsid protein annealing of a primer-template enhances (+)-strand DNA synthesis and fidelity by HIV-1 reverse transcriptase. J. Mol. Biol. 415, 866–880.

Kirby, K.A., Michailidis, E., Fetterly, T.L., Steinbach, M.A., Singh, K., Marchand, B., Leslie, M.D., Hagedorn, A.N., Kodama, E.N., Marquez, V.E., Hughes, S.H., Mitsuya, H., Parniak, M.A., Sarafianos, S.G., 2013. Effects of substitutions at the 4′ and 2 positions on the bioactivity of 4′-ethynyl-2-fluoro-2′-deoxyadenosine. Antimicrob. Agents Chemother. 57, 6254–6264.

Kirby, K.A., Singh, K., Michailidis, E., Marchand, B., Kodama, E.N., Ashida, N., Mitsuya, H., Parniak, M.A., Sarafianos, S.G., 2011. The sugar ring conformation of 4′-ethynyl-2-fluoro-2′-deoxyadenosine and its recognition by the polymerase active site of HIV reverse transcriptase. Cell. Mol. Biol. (Noisy-le-Grand) 57, 40–46.

Michailidis, E., Marchand, B., Kodama, E.N., Singh, K., Matsuoka, M., Kirby, K.A., Ryan, E.M., Sawani, A.M., Nagy, E., Ashida, N., Mitsuya, H., Parniak, M.A., Sarafianos, S.G., 2009. Mechanism of inhibition of HIV-1 reverse transcriptase by 4′-ethynyl-2-fluoro-2′-deoxyadenosine triphosphate, a translocation-defective reverse transcriptase inhibitor. J. Biol. Chem. 284, 35681–35691.

Michailidis, E., Ryan, E.M., Hachiya, A., Kirby, K.A., Marchand, B., Leslie, M.D., Huber, A.D., Ong, Y.T., Jackson, J.C., Singh, K., Kodama, E.N., Mitsuya, H., Parniak, M.A., Sarafianos, S.G., 2013. Hypersusceptibility mechanism of Tenofovir-resistant HIV to EFdA. Retrovirology 10, 65.

Mullins, J.I., Heath, L., Hughes, J.P., Kicha, J., Styrchak, S., Wong, K.G., Rao, U., Hansen, A., Harris, K.S., Laurent, J.P., Li, D., Simpson, J.H., Essigmann, J.M., Loeb, L.A., Parkins, J., 2011. Mutation of HIV-1 genomes in a clinical population treated with the mutagenic nucleoside KP1461. PLoS One 14, e15135.

Murakami, E., Basavapathruni, A., Bradley, W.D., Anderson, K.S., 2005. Mechanism of action of a novel viral mutagenic covert nucleotide: molecular interactions with HIV-1 reverse transcriptase and host cell DNA polymerases. Antiviral Res. 67, 10–17.

Nakata, H., Amano, M., Koh, Y., Kodama, E., Yang, G., Bailey, C.M., Kohgo, S., Hayakawa, H., Matsuoka, M., Anderson, K.S., Cheng, Y.C., Mitsuya, H., 2007. Activity against human immunodeficiency virus type 1, intracellular metabolism, and effects on human DNA polymerases of 4′-ethynyl-2-fluoro-2′-deoxyadenosine. Antimicrob. Agents Chemother. 51, 2701–2708.

Ohrui, H., Kohgo, S., Hayakawa, H., Kodama, E., Matsuoka, M., Nakata, T., Mitsuya, H., 2007. 2′-Deoxy-4′-C-ethynyl-2-fluoroadenosine: a nucleoside reverse transcriptase inhibitor with highly potent activity against wide spectrum of HIV-1 strains, favorable toxic profiles, and stability in plasma. Nucleosides Nucleotides Nucleic Acids 26, 1543–1546.

Ray, A.S., Basavapathruni, A., Anderson, K.S., 2002. Mechanistic studies to understand the progressive development of resistance in human immunodeficiency virus type 1 reverse transcriptase to abacavir. J. Biol. Chem. 277, 40479–40490.

Sohl, C.D., Kasiviswanathan, R., Kim, J., Pradere, U., Schinazi, R.F., Copeland, W.C., Mitsuya, H., Baba, M., Anderson, K.S., 2012a. Balancing antiviral potency and host toxicity: identifying a nucleotide inhibitor with an optimal kinetic phenotype for HIV-1 reverse transcriptase. Mol. Pharmacol. 82, 125–133.

Sohl, C.D., Singh, K., Kasiviswanathan, R., Copeland, W.C., Mitsuya, H., Sarafianos, S.G., Anderson, K.S., 2012b. Mechanism of interaction of human mitochondrial DNA polymerase gamma with the novel nucleoside reverse transcriptase inhibitor 4′-ethynyl-2-fluoro-2′-deoxyadenosine indicates a low potential for host toxicity. Antimicrob. Agents Chemother. 56, 1630–1634.

Sohl, C.D., Kasiviswanathan, R., Copeland, W.C., Anderson, K.S., 2013. Mutations in human DNA polymerase gamma confer unique mechanisms of catalytic deficiency that mirror the disease severity in mitochondrial disorder patients. Hum. Mol. Genet. 22, 1074–1085.

Tchesnokov, E.P., Obikhod, A., Schinazi, R.F., Gotte, M., 2008. Delayed chain termination protects the anti-hepatitis B virus drug entecavir from excision by HIV-1 reverse transcriptase. J. Biol. Chem. 283, 34218–34228.

Vaccaro, J.A., Parnell, K.M., Terezakis, S.A., Anderson, K.S., 2000. Mechanism of inhibition of the human immunodeficiency virus type 1 reverse transcriptase by d4TTP: an equivalent incorporation efficiency relative to the natural substrate dTTP. Antimicrob. Agents Chemother. 44, 217–221.

Zhang, W., Parniak, M.A., Mitsuya, H., Sarafianos, S.G., Graebing, P.W., Rohan, L.C., 2013. Preformulation studies of EFdA, a novel nucleoside reverse transcriptase inhibitor for HIV prevention. Drug Dev. Ind. Pharm.. http://dx.doi.org/10.3109/03639045.2013.809535.

THE JOURNAL OF BIOLOGICAL CHEMISTRY VOL. 289, NO. 35, pp. 24533–24548, August 29, 2014
Published in the U.S.A.

4′-Ethynyl-2-fluoro-2′-deoxyadenosine (EFdA) Inhibits HIV-1 Reverse Transcriptase with Multiple Mechanisms*

Received for publication, March 3, 2014, and in revised form, June 17, 2014 Published, JBC Papers in Press, June 26, 2014, DOI 10.1074/jbc.M114.562694

Eleftherios Michailidis,[a,b] Andrew D. Huber,[a,c] Emily M. Ryan,[a,b] Yee T. Ong,[a,b] Maxwell D. Leslie,[a,b] Kayla B. Matzek,[a,b] Kamalendra Singh,[a,b] Bruno Marchand,[a,b1] Ariel N. Hagedorn,[a,b] Karen A. Kirby,[a,b] Lisa C. Rohan,[d,e] Eiichi N. Kodama,[f2] Hiroaki Mitsuya,[g,h2] Michael A. Parniak,[i] and Stefan G. Sarafianos[a,b,j3]

From the [a]Christopher Bond Life Sciences Center and Departments of [c]Veterinary Pathobiology and [j]Biochemistry, University of Missouri, Columbia, Missouri 65211, [b]Department of Molecular Microbiology and Immunology, University of Missouri School of Medicine, Columbia, Missouri 65211, [d]Magee-Womens Research Institute and [e]Department of Pharmaceutical Sciences, School of Pharmacy, University of Pittsburgh, Pittsburgh, Pennsylvania 15213, [f]Division of Emerging Infectious Diseases, Tohoku University, Sendai 980-8575, Japan, [g]Department of Internal Medicine, Kumamoto University, Kumamoto 860-8556, Japan, [h]Experimental Retrovirology Section, HIV/AIDS Malignancy Branch, National Institutes of Health, Bethesda, Maryland 20892, and [i]Department of Microbiology and Molecular Genetics, University of Pittsburgh School of Medicine, Pittsburgh, Pennsylvania 15219

Background: 4′-Ethynyl-2-fluoro-2′-deoxyadenosine (EFdA) is a highly potent nucleoside analog reverse transcriptase (RT) inhibitor with a 3′-OH.
Results: EFdA inhibits RT as an immediate or delayed chain terminator depending on the DNA substrate sequence. RT efficiently misincorporates EFdA, producing non-extendable mismatched primers protected from excision.
Conclusion: EFdA blocks RT by multiple mechanisms.
Significance: Understanding the EFdA inhibition mechanism will help develop better antivirals.

4′-Ethynyl-2-fluoro-2′-deoxyadenosine (EFdA) is a nucleoside analog that, unlike approved anti-human immunodeficiency virus type 1 (HIV-1) nucleoside reverse transcriptase inhibitors, has a 3′-OH and exhibits remarkable potency against wild-type and drug-resistant HIVs. EFdA triphosphate (EFdA-TP) is unique among nucleoside reverse transcriptase inhibitors because it inhibits HIV-1 reverse transcriptase (RT) with multiple mechanisms. (*a*) EFdA-TP can block RT as a translocation-defective RT inhibitor that dramatically slows DNA synthesis, acting as a *de facto* immediate chain terminator. Although non-translocated EFdA-MP-terminated primers can be unblocked, they can be efficiently converted back to the EFdA-MP-terminated form. (*b*) EFdA-TP can function as a delayed chain terminator, allowing incorporation of an additional dNTP before blocking DNA synthesis. In such cases, EFdA-MP-terminated primers are protected from excision. (*c*) EFdA-MP can be efficiently misincorporated by RT, leading to mismatched primers that are extremely hard to extend and are also protected from excision. The context of template sequence defines the relative contribution of each mechanism and affects the affinity of EFdA-MP for potential incorporation sites, explaining in part the lack of antagonism between EFdA and tenofovir. Changes in the type of nucleotide before EFdA-MP incorporation can alter its mechanism of inhibition from delayed chain terminator to immediate chain terminator. The versatility of EFdA in inhibiting HIV replication by multiple mechanisms may explain why resistance to EFdA is more difficult to emerge.

The enzyme reverse transcriptase (RT) of human immunodeficiency virus type 1 (HIV-1)[4] has been the major target of antiretrovirals that belong to two general classes referred to as nucleoside RT inhibitors (NRTIs) and non-nucleoside RT inhibitors. Currently there are eight approved NRTIs for the treatment of HIV infection, and these are almost always components of first line therapies (1–8). Once phosphorylated, NRTI triphosphates compete with the natural dNTPs for incorporation into the viral nascent DNA chain, and because they lack a 3′-OH, they inhibit further DNA polymerization by acting as chain terminators. Despite the availability of potent antivirals, HIV can escape treatment by developing drug resistance mutations. Thus, there is a need for potent drugs that block wild-type and drug-resistant HIVs.

We have shown previously that nucleoside analogs that retain the 3′-OH group and have a modification at the 4′-position of the sugar ring can inhibit HIV-1 RT very efficiently (9).

* This work was supported, in whole or in part, by National Institutes of Health Grants R01AI076119, R01AI076119-S1, R01AI076119-02S1, R01AI099284, R01AI100890, R21AI112417, and P01GM103368 (to S. G. S.) and AI079801 (to M. A. P.). This work was also supported by Mizzou Advantage and the Ministry of Knowledge and Economy, Bilateral International Collaborative Research and Development Program, Republic of Korea. Co-authors Drs. Hiroaki Mitsuya and Eiichi N. Kodama are inventors of EFdA, and thus there is a potential conflict of interest.

[1] Present Address: Gilead Sciences Inc., Foster City, CA 94404.
[2] Co-inventors of EFdA.
[3] To whom correspondence should be addressed: Christopher Bond Life Sciences Center, Depts. of Molecular Microbiology and Immunology and Biochemistry, University of Missouri, Columbia, MO 65211. Tel.: 573-882-4338; Fax: 573-884-9676; E-mail: sarafianoss@missouri.edu.

[4] The abbreviations used are: HIV-1, human immunodeficiency virus type 1; NRTI, nucleoside RT inhibitor; EFdA, 4′-ethynyl-2-fluoro-2′-deoxyadenosine; TFV, tenofovir; MP, monophosphate; DP, diphosphate; TP, triphosphate; T/P, template/primer; ICT, immediate chain terminator; DCT, delayed chain terminator; SPR, surface plasmon resonance; N-site, nucleotide-binding or pre-translocation site; P-site, primer-binding or post-translocation site.

We also reported that 4′-ethynyl-2-fluoro-2′-deoxyadenosine (EFdA) is a deoxyadenosine analog with anti-HIV efficacy at subnanomolar concentrations in primary cells, making it the most potent NRTI described to date (10–13). Unlike all approved anti-HIV NRTIs, EFdA possesses a 3′-OH, which mimics the structure of normal dNTPs (see Fig. 1*A*). It has been demonstrated that this property provides enhanced phosphorylation of the NRTIs by cellular kinases increasing their antiviral efficacy (14). In addition, EFdA has 4′-ethynyl and 2-fluoro substitutions, which also contribute to its extraordinary selectivity index of about 200,000 as determined after initial antiviral characterization of a series of 4′-substituted analogs (9, 11). We have shown that EFdA is resistant to degradation by adenosine deaminase, providing an enhanced half-life to the compound compared with other NRTIs (11, 15). EFdA is very effective not only against wild-type HIV but also against drug-resistant strains and has displayed synergistic antiviral effects when combined with other inhibitors such as the recently approved second generation non-NRTI rilpivirine (16). We have also shown that EFdA is significantly better than tenofovir (TFV), zidovudine, and emtricitabine in blocking simian immunodeficiency virus replication in monkey peripheral blood mononuclear cells and that it was highly effective at treating simian immunodeficiency virus infection and AIDS symptoms in simian immunodeficiency virus-infected macaques with advanced AIDS with no apparent signs of toxicity (17).

Here we used a series of biochemical experiments and demonstrated that EFdA triphosphate (EFdA-TP) blocks RT with multiple mechanisms. Specifically, we found that, unlike approved anti-HIV NRTIs, EFdA-TP can act as a *de facto* immediate or delayed chain terminator in a manner that depends on the sequence of the nucleic acid template. Moreover, EFdA monophosphate (EFdA-MP) is misincorporated by RT, resulting in mismatched primers that are very difficult to extend. Finally, the detailed analysis of the versatile mechanisms of RT inhibition by EFdA provides novel insights into a reduced resistance profile for EFdA because delayed termination seems to protect EFdA-MP-terminated primers from excision.

EXPERIMENTAL PROCEDURES

Enzymes, Nucleic Acids, Nucleotides, and Nucleotide Analogs

HIV-1 RT was expressed and purified as described previously (10, 18–23). RT was expressed in JM-109 cells (Invitrogen) and purified by nickel affinity chromatography and Mono Q anion exchange chromatography (24). Oligonucleotides used in this study were chemically synthesized and purchased from Integrated DNA Technologies (Coralville, IA). Sequences of the DNA substrates are shown in Table 1. Deoxynucleotide triphosphates and dideoxynucleotide triphosphates were purchased from Fermentas (Glen Burnie, MD). Concentrations of nucleotides were calculated spectrophotometrically on the basis of absorption at 260 nm and their extinction coefficients. All nucleotides were treated with inorganic pyrophosphatase (Roche Diagnostics) as described previously (25) to remove traces of PP_i contamination that might interfere with the rescue assay.

Active Site Titration of HIV-1 RT

To determine polymerization-competent RT populations used in this study, we first carried out active site titration assays using pre-steady state experiments (26, 27). A fixed concentration of RT (50 nM; determined by absorbance measurements) in RT buffer (50 mM NaCl and 50 mM Tris-HCl, pH 7.8) was incubated with increasing concentrations of template/primer (T/P; T_{d31}/P_{d18} where T_{d31} is the DNA template of 31 nucleotides in length annealed to P_{d18}, which is a DNA primer of 18 nucleotides in length) followed by rapidly mixing with a solution containing 5 mM $MgCl_2$ and 50 μM dATP in the same RT buffer using a rapid quench-flow instrument (RQF-3, KinTek Corp., Austin, TX) at 37 °C for 0.005–1 s. The reactions were quenched by the addition of 150 mM EDTA. The products were resolved on 15% polyacrylamide and 7 M urea gels. In this and in subsequent assays, the gels were scanned with a Typhoon FLA 9000 phosphorimaging system (GE Healthcare), and densitometry analysis was performed using ImageQuant TL software (GE Healthcare). The amounts of extended primer (*P*) were plotted against time, and the data were fit to a biphasic equation (Equation 1) using GraphPad Prism 4.0 (GraphPad Software Inc., La Jolla, CA) (26),

$$P = A(1 - e^{-k_{obs}t}) + k_{ss}t \quad \text{(Eq. 1)}$$

where *A* is the amplitude of the burst phase that represents the E-DNA complex at the start of the reaction, k_{obs} is the observed burst rate constant for dNTP incorporation, k_{ss} corresponds to the steady state rate constant, and *t* is the reaction time. Next, the active site concentration and T/P dissociation constant ($K_{d(DNA)}$) were determined by plotting the amplitude (*A*) against T/P concentration. The data were fit by non-linear regression to a quadratic equation,

$$A = 0.5((K_{d(DNA)} + [RT] + [DNA]) - \sqrt{0.25(K_{d(DNA)} + [RT] + [DNA])^2 - ([RT][DNA])}) \quad \text{(Eq. 2)}$$

where [RT] is the concentration of actively binding polymerase molecules. Subsequent pre-steady state experiments were performed using corrected active site concentrations.

Gel-based Drug Susceptibility Assays: Inhibition of HIV-1 RT-catalyzed DNA Synthesis by EFdA-TP and ddATP

DNA template was annealed to 5′-Cy3-labeled DNA primer at a 3:1 molar ratio. For these experiments, we used T_{d31}/P_{d18} and T_{d26}/P_{d18+5} where P_{d18+5} is an 18-mer DNA primer shifted by five nucleotides relative to the P_{d18} primer. Throughout most of our work, we carried out our analyses using two types of primers (in this case, P_{d18} and P_{d18+5}) that allowed us to interrogate two different template sites where RT incorporates dAMP or EFdA-MP at different affinities and different translocation efficiencies. To monitor primer extension, the DNA/DNA hybrid (20 nM) was incubated at 37 °C with RT (20 nM) in RT buffer. Varying amounts of EFdA-TP or ddATP were added, and the reactions were initiated by the addition of 6 mM $MgCl_2$ in a final volume of 20 μl. All dNTPs were present at a final concentration of 10 μM. The reactions were terminated after 15 min by adding an equal volume of 100% formamide containing

traces of bromophenol blue. The products were resolved on a 15% polyacrylamide and 7 M urea gel and analyzed as described before (10, 22, 23).

Effect of Template Sequence on RT Inhibition by EFdA-TP

Various T/Ps (oligonucleotide sequences are shown in Table 1) were used to determine the effect of the DNA sequence on the mechanism of inhibition by EFdA-TP. The experiments were carried out as described above.

Surface Plasmon Resonance Assays

Surface plasmon resonance (SPR) was used to determine the kinetic constants of nucleotide triphosphate or EFdA-TP binding to HIV-1 RT. To allow nucleotide binding to the reverse transcriptase, the enzyme was covalently cross-linked to a double-stranded DNA/DNA T/P as described before (24). Briefly, a thiol-modified DNA primer at the N^2 position of a guanosine residue (indicated by *X* in 5′-ACAGTCCCTGTTCGG*X*C-GCG-3′) was heat-annealed to a 5′-biotinylated DNA template (5′-biotin-TAGATCAGTCATGCTCCGCGCCCGAACAGGG-ACTGTG) at a 3:1 T/P ratio (Table 1). The double-stranded DNA was cross-linked to RT containing mutation Q258C by incubating overnight at 30 °C in a mixture containing 25 mM Tris, pH 7.8, 75 mM NaCl, 10 mM $MgCl_2$, and 100 μM ddGTP. The incorporation of the dideoxynucleotide into the T/P (DNA_{ddGMP}) aligns the thiol-modified G with the cysteine 258 of RT and allows disulfide bond formation as we have previously described (24). The covalent RT-DNA_{ddGMP} complex was purified by tandem nickel affinity/ion exchange chromatography to remove unreacted DNA and enzyme (28). The purified complex was immobilized on a streptavidin sensor chip on a Biacore T100 system (GE Healthcare). RT-DNA_{ddGMP} was flowed over the chip surface of channel 2 until ~8,000 response units were immobilized through the very strong interactions of the biotinylated RT-DNA_{ddGMP} with the streptavidin sensor chip. Channel 1 was left untouched and was later used as a control surface. Increasing concentrations of dATP (1–1,000 nM) or EFdA-TP (5–1,000 nM) were flowed in channels 1 and 2 in RT buffer and 10 mM $MgCl_2$ for 2 min to allow nucleotide association and dissociation. The signal observed in channel 1 (control channel) was subtracted from the signal obtained from the RT-DNA_{ddGMP} channel 2. The ddGTP at the 3′-end of the DNA primer prevents incorporation of the dATP or EFdA-TP and allows estimation of their dissociation and association rates, the ratio of which provides the K_d equilibrium binding constant of the binding of the incoming nucleotide triphosphate to the RT-DNA_{ddGMP} complex. Optimal analysis of the binding signal was performed using a two-state reaction protocol that assumes a conformational change associated with substrate binding in the Biacore T100 software to obtain measured kinetic constants. Specifically, the overall equilibrium dissociation constant K_d for this type of two-state reaction protocol is defined by $(k_{d1}/k_{a1})\cdot(k_{d2}/(k_{d2} + k_{a2}))$ where k_{a1} is the association rate constant for substrate binding, k_{d1} is the dissociation rate constant for substrate from the complex, k_{a2} is the forward rate constant for the conformational change, and k_{d2} is the reverse rate constant for the conformational change.

Pre-steady State Kinetics of dATP and EFdA-TP Incorporation

Pre-steady state kinetics analysis was performed using dATP or EFdA-TP single nucleotide incorporation experiments catalyzed by RT. The optimal rate of polymerization (k_{pol}) was determined using the rapid quench-flow method as described before (19, 26, 27, 29). Specifically, a solution containing 50 nM RT and 50 nM T_{d31}/P_{d18} or T_{d26}/P_{d18+5} in RT buffer was rapidly mixed with a solution of 5 mM $MgCl_2$ and 1–50 μM dATP or EFdA-TP for reaction times ranging between 0.005 and 2 s followed by quenching with 150 mM EDTA. The reaction products were resolved and quantified as described above. The observed burst rates (k_{obs}) at each dATP or EFdA-TP concentration were determined by fitting the data to Equation 1 and solving the equation by non-linear regression using GraphPad Prism 4.0.

To determine the optimal rates of dATP and EFdA-TP incorporation (k_{pol}) and their binding to the enzyme-DNA complex ($K_{d(dATP)}$ or $K_{d(EFdA\text{-}TP)}$), observed burst rates (k_{obs}) were fit to the following hyperbolic equation.

$$k_{obs} = (k_{pol}[dNTP])/(K_{d(dNTP)} + [dNTP]) \quad \text{(Eq. 3)}$$

All experiments were carried out independently at least two times, and the standard deviations of the kinetic parameters are reported in the respective tables.

Pre-steady State Kinetics of dATP and EFdA-TP Misincorporation

We used pre-steady state kinetics to monitor the misincorporation of dAMP and EFdA-MP opposite an A template base using the $T_{d31(1A)}/P_{d18}$ or $T_{d31(6A)}/P_{d18+5}$ template/primer, which has an A at the first template overhang position when P_{d18} or P_{d18+5} was used as the primer, respectively (DNA sequences are shown in Table 1). We used both P_{d18} and P_{d18+5} primers to interrogate potential differences in misincorporation efficiency at two template sites where substrates are incorporated at different efficiencies. Similarly, we monitored misincorporation of dATP and EFdA-TP opposite *G* using $T_{d31(1G)}/P_{d18}$ or $T_{d31(6G)}/P_{d18+5}$ and misincorporation opposite a C using $T_{d31(1C)}/P_{d18}$ or $T_{d31(6C)}/P_{d18+5}$. In these experiments, a solution containing 30 nM RT and a 20 nM concentration of the corresponding T/P in RT buffer was mixed with a solution of 6 mM $MgCl_2$ and various concentrations of dATP or EFdA-TP for the indicated reaction times followed by quenching with an equal volume of formamide. The reaction products were resolved and quantified as described above. Further analysis was carried out as described for the match pre-steady state kinetics experiments.

Site-specific Fe^{2+} Footprinting Assays

Site-specific Fe^{2+} footprints were monitored on 5′-Cy3-labeled DNA templates. 100 nM 5′-Cy3-T_{d43}/P_{d30} or 5′-Cy3-T_{d43}/P_{d30+5} was incubated with 600 nM RT in a buffer containing 120 mM sodium cacodylate, pH 7.0, 20 mM NaCl, 6 mM $MgCl_2$, and 1 μM EFdA-TP or 5 μM ddATP to allow quantitative chain termination. Prior to treatment with Fe^{2+}, complexes were preincubated for 7 min with increasing concentrations of the next incoming nucleotide (dTTP). The complexes were treated with ammonium iron sulfate (1 mM) as

described previously (10, 30). This reaction relies on autoxidation of Fe^{2+} (31) to create a local concentration of hydroxyl radicals that cleave the DNA at the nucleotide closest to the Fe^{2+} specifically bound to the RNase H active site. The two types of T/P systems carrying P_{d18} and P_{d18+5} primers allowed us to interrogate the translocation efficiencies in different nucleic acid sequence contexts.

Extension of EFdA-MP-terminated Primers

$T_{d31}/P_{d18\text{-}EFdA\text{-}MP}$ (chemically prepared T/P possessing EFdA-MP at the 3′-end of the primer) and $T_{d26}/P_{d18+5\text{-}EFdA\text{-}MP}$ were prepared by incubating 1 μM EFdA-TP, a 1 μM concentration of the corresponding T/P, 1 μM RT, and 6 mM $MgCl_2$ in RT buffer. The reactions were carried out at 37 °C for 1 h. Similarly, for the extension of the mismatched primers, $T_{d31(6C)}/P_{d18+5\text{-}EFdA\text{-}MP}$, $T_{d31(6G)}/P_{d18+5\text{-}EFdA\text{-}MP}$, and $T_{d31(6A)}/P_{d18+5\text{-}EFdA\text{-}MP}$ were prepared by incubating 20 μM EFdA-TP, a 1 μM concentration of the corresponding T/P, 2 μM RT, and 6 mM $MgCl_2$ in RT buffer. The reactions were carried out at 37 °C for 4 h. After incorporation of EFdA-MP, the various $T/P_{EFdA\text{-}MP}$ substrates were purified using the QIAquick nucleotide removal kit (Qiagen, Valencia, CA). Under these conditions, the extension of T/P to $T/P_{EFdA\text{-}MP}$ was complete. Purified $T_{d31}/P_{d18\text{-}EFdA\text{-}MP}$, $T_{d26}/P_{d18+5\text{-}EFdA\text{-}MP}$, $T_{d31(6C)}/P_{d18+5\text{-}EFdA\text{-}MP}$, $T_{d31(6G)}/P_{d18+5\text{-}EFdA\text{-}MP}$, or $T_{d31(6A)}/P_{d18+5\text{-}EFdA\text{-}MP}$ (5 nM) was incubated with 20 nM RT in RT buffer and 6 mM $MgCl_2$. The first incoming nucleotide was added at different concentrations (0–50 μM) in the presence of the other dNTPs (1 μM). The reactions were incubated at 37 °C for 5 and 30 min, and products were analyzed as described above.

Pre-steady State Kinetics of dTTP Incorporation to $T/P_{EFdA\text{-}MP}$

Pre-steady state kinetics analysis of dTTP incorporation to $T/P_{EFdA\text{-}MP}$ was performed using $T_{d31}/P_{d18\text{-}EFdA\text{-}MP}$, $T_{d26}/P_{d18+5\text{-}EFdA\text{-}MP}$, or $T_{d26(5C)}/P_{d18+5(5G)\text{-}EFdA\text{-}MP}$. In these experiments, a solution containing 30 nM RT and a 20 nM concentration of the corresponding T/P in RT buffer was mixed with a solution of 6 mM $MgCl_2$ and various concentrations of dTTP for 30 s to 10 min followed by quenching with an equal volume of formamide. The reaction products were resolved and quantified as described above. Further analysis was carried out as described for the match pre-steady state kinetics experiments.

PP_i- and ATP-dependent Excision and Rescue of $T/P_{EFdA\text{-}MP}$

PP_i-dependent Excision of $T/P_{EFdA\text{-}MP}$—$T_{d26}/P_{d18+5\text{-}EFdA\text{-}MP\text{-}dTMP}$ was prepared similarly to $T_{d26}/P_{d18+5\text{-}EFdA\text{-}MP}$. After EFdA-MP incorporation, 100 μM dTTP was added to the reaction and incubated at 37 °C for an additional 1 h. The purification of the terminated primer was performed as described before. 20 nM purified $T_{d31}/P_{d18\text{-}EFdA\text{-}MP}$ or $T_{d26}/P_{d18+5\text{-}EFdA\text{-}MP\text{-}dTMP}$ was incubated at 37 °C with 60 nM RT in the presence of 150 μM PP_i in RT buffer and 6 mM $MgCl_2$. Aliquots of the reaction were stopped at different times (0–30 min) and analyzed as described above.

ATP-dependent Rescue of $T/P_{EFdA\text{-}MP}$—20 nM purified $T_{d31}/P_{d18\text{-}EFdA\text{-}MP}$ was incubated with 60 nM RT in the presence of 3.5 mM ATP, 100 μM dATP, 0.5 μM dTTP, and 10 μM ddGTP in RT buffer and 10 mM $MgCl_2$. Similarly, 20 nM purified $T_{d26}/P_{d18+5\text{-}EFdA\text{-}MP+dTMP}$ was incubated with 60 nM RT in the presence of 3.5 mM ATP, 100 μM dTTP, and 10 μM ddCTP in RT buffer and 10 mM $MgCl_2$. Reactions were arrested at various time points (0–90 min) and analyzed as described above. Control reactions without dNTPs and ATP (no excision; no incorporation) or without ATP (no excision; incorporation) were incubated for the maximum time (90 min).

PP_i-dependent Excision of $T/P_{EFdA\text{-}MP}$ in Which EFdA-MP Is Incorporated as a Match or Mismatch—20 nM purified $T_{d31(6X)}/P_{d18+5\text{-}EFdA\text{-}MP}$ (where X = T, A, C, or G) was incubated at 37 °C with 60 nM RT in the presence of 150 μM PP_i in RT buffer and 6 mM $MgCl_2$. Aliquots of the reaction were stopped at different times (0–20 min) and analyzed as described above.

EFdA and Tenofovir Combination Studies: Inhibition of HIV-1 RT-catalyzed DNA Synthesis and Stopping Patterns by EFdA-TP and TFV-DP

We monitored primer extension using two T/P systems. (*a*) A shorter T/P, $T_{d31(7C)}/P_{d18}$ (20 nM), was incubated at 37 °C with RT (20 nM) in RT buffer. Varying amounts of EFdA-TP (0–8 μM) and tenofovir diphosphate (TFV-DP; 0–2 μM) were added, and the reactions were initiated by the addition of 6 mM $MgCl_2$ in a final volume of 20 μl. All dNTPs were present at a final concentration of 1 μM. The reactions were terminated after 15 min by adding an equal volume of 100% formamide containing traces of bromophenol blue. The products were analyzed as described above. (*b*) Using a longer template, we compared the stopping patterns of EFdA-TP and TFV-DP. Specifically, $T_{d100}/P_{d18(100)}$ (50 nM) was incubated at 37 °C with RT (20 nM) in RT buffer, 6 mM $MgCl_2$, 1 μM dNTPs, and 240 nM EFdA-TP or 2 μM TFV-DP. The reactions were terminated after 15 min by adding an equal volume of 100% formamide containing traces of bromophenol blue, and the products were analyzed as described above.

RESULTS

EFdA-TP Inhibits RT with Multiple Mechanisms: EFdA-TP Inhibits RT Primarily as an Effective Immediate or Delayed Chain Terminator (ICT or DCT)—All NRTIs approved for the treatment of HIV infection mimic the natural dNTPs, but because they lack a 3′-OH group, once incorporated into the nascent DNA they act as immediate (or obligate) chain terminators. Primer extension assays show that despite having a 3′-OH EFdA-TP inhibits RT-catalyzed DNA synthesis mainly at the point of incorporation as a *de facto* ICT, similar to other ICTs such as ddATP (Fig. 1*B*; strong stops at positions of incorporation P1 and to a lesser extent at P10). For the sake of simplicity, we use the term "immediate chain terminator" in lieu of the more accurate "*de facto* immediate chain terminator" as EFdA-TP causes a dramatic but not 100% complete suppression of primer extension (eventually some primer extension can be observed at high dNTP concentrations).

However, our data show that EFdA-TP can also inhibit RT as a DCT. Specifically, our primer extension assays revealed additional bands that do not correspond to positions where EFdA-TP or other dATP analogs are expected to be incorporated. Hence, there are strong bands at positions P7 and to a

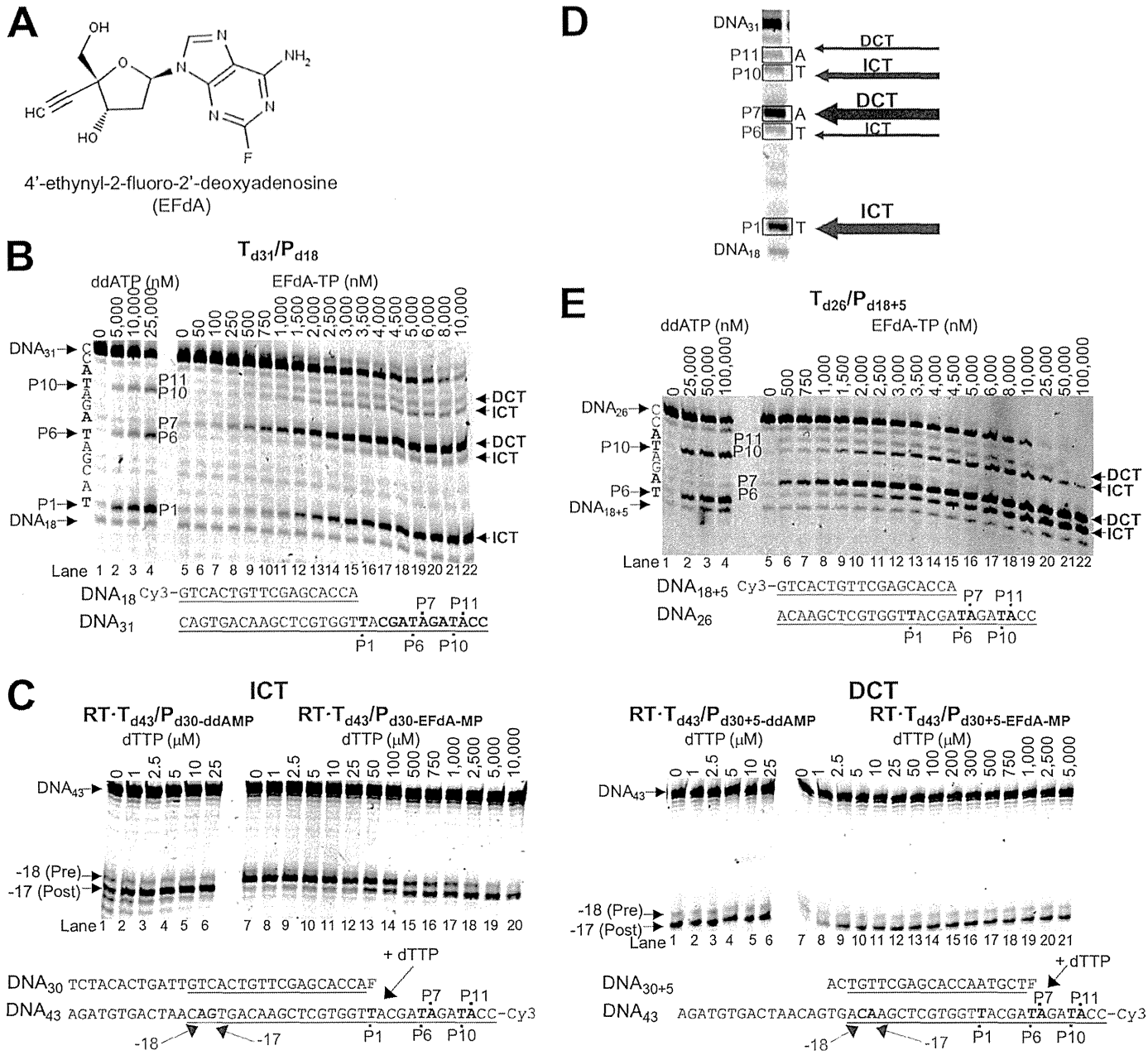

FIGURE 1. **EFdA-TP inhibits RT-catalyzed DNA synthesis as an ICT or DCT.** *A*, structure of EFdA. *B*, DNA/DNA T_{d31}/P_{d18} (20 nM) was incubated with 20 nM RT for 15 min in the presence of 10 μM dNTPs, 6 mM $MgCl_2$, and increasing concentrations of ddATP (*lanes 1–4*) or EFdA-TP (*lanes 5–22*). The sequence of the template and the mechanism that EFdA-TP uses to inhibit RT are shown next to different bands of the gel. *C*, the translocation state of RT after ddAMP (*lanes 1–6* in both gels) or EFdA-MP (*lanes 7–20* and *7–21*) incorporation was determined using site-specific Fe^{2+} footprinting. T_{d43}/P_{d30} or T_{d43}/P_{d30+5} (100 nM) with 5′-Cy3-label on the DNA templates was incubated with 600 nM RT and various concentrations of the next incoming nucleotide (dTTP). The complexes were treated for 5 min with 1 mM ammonium iron sulfate. An excision at position −18 indicates a pre-translocation complex, whereas the one at position −17 represents a post-translocation complex. The sequences of the T/Ps that were used in the experiments are shown under the gels with *underlined* matched sequences in primer extension and footprinting assays. *D*, representative reactions that highlight the sites on the template sequences where EFdA-TP acts as an ICT or DCT. The *numbers* indicate the points (marked in *red*) of the dATP or dATP analog incorporation (P1, P6, and P10). In *green* color, we indicate the bases after dATP or dATP analog incorporation (P7 and P11). *E*, similar to *A*, the effect of ddATP and EFdA-TP on primer extension was observed using the DNA/DNA T_{d31}/P_{d18+5}.

lesser extent at P11, suggesting that EFdA-TP can act as a DCT primarily when incorporated at P6 and to a lesser extent at P10. In these cases after RT incorporates EFdA-MP at the P6 and P10 positions, it continues incorporating the next dNTP before DNA synthesis is stalled. We confirmed these findings using an oligonucleotide substrate with a shorter template but longer primer sequence that allowed examination of EFdA-MP incorporation only at the P6 and P10 sites (T_{d26}/P_{d18+5}; Fig. 1*E*). Hence, EFdA-TP acts exclusively as an ICT at P1 and mostly as an ICT at P10, whereas it acts primarily as a DCT at P6 and to a lesser extent at P10 (Fig. 1, *B* and *E*). Using hydroxyl radical footprinting assays of RT bound to an EFdA-MP-terminated T/P ($T/P_{EFdA\text{-}MP}$) we demonstrated a correlation of ICT inhibition (such as at P1 site) and a decreased translocation of RT from the nucleotide-binding or pre-translocation site (N-site; cleavage at −18) to the primer-binding or post-translocation

TABLE 1

DNA oligonucleotide sequences used in this study

An example of the oligonucleotide abbreviation is as follows: $T_{d31(2T)}/P_{d18}$, template DNA of 31 nucleotides in length with a T in the second unpaired position after annealing to the corresponding 18-mer DNA primer. The bases that vary in similar sequences are marked in red. P_{d18+5} is a primer that is annealed on a template five nucleotides further than P_{d18}. In each group of templates, the varying base is indicated inside parentheses: $T_{d31(6G)}$. For the SPR experiments, a thiol-modified DNA primer containing a disulfide on the N^2 of a guanosine residue is indicated by X in the sequence. Cy3 or biotin labels are indicated next to the sequences.

Polymerization assays	
T_{d100}	5′TAG TGT GTG CCC GTC TGT TGT GTG ACT CTG GTA ACT AGA GAT CCC TCA GAC CCT TTT AGT CAG TGT GGA AAA TCT CTA GCA GTG GCG CCC GAA CAG GGA C
$P_{d18(100)}$	5′GTC CCT GTT CGG GCG CCA
T_{d31} [=$T_{d31(0T/2A/5A/6T/7A)}$]	5′CCA TAG ATA GCA TTG GTG CTC GAA CAG TGA C
P_{d18}	5′Cy3 GTC ACT GTT CGA GCA CCA
$T_{d31(0A)}$	5′CCA TAG ATA GCA TAG GTG CTC GAA CAG TGA C
$T_{d31(0C)}$	5′CCA TAG ATA GCA TCG GTG CTC GAA CAG TGA C
$T_{d31(0G)}$	5′CCA TAG ATA GCA TGG GTG CTC GAA CAG TGA C
$P_{d18(0T)}$	5′Cy3 GTC ACT GTT CGA GCA CCT
$P_{d18(0G)}$	5′Cy3 GTC ACT GTT CGA GCA CCG
$P_{d18(0C)}$	5′Cy3 GTC ACT GTT CGA GCA CCC
P_{d17}	5′Cy3 GTC ACT GTT CGA GCA CC
$T_{d31(2T)}$	5′CCA TAG ATA GCT TTG GTG CTC GAA CAG TGA C
$T_{d31(2C)}$	5′CCA TAG ATA GCC TTG GTG CTC GAA CAG TGA C
$T_{d31(2G)}$	5′CCA TAG ATA GCG TTG GTG CTC GAA CAG TGA C
$T_{d31(7T)}$	5′CCA TAG TTA GCG TTG GTG CTC GAA CAG TGA C
$T_{d31(7C)}$	5′CCA TAG CTA GCG TTG GTG CTC GAA CAG TGA C
$T_{d31(7G)}$	5′CCA TAG GTA GCG TTG GTG CTC GAA CAG TGA C
$T_{d31(5T)}$ [=$T_{d31(4G5T)}$]	5′CCA TAG ATT GCA TTG GTG CTC GAA CAG TGA C
$T_{d31(4C5T)}$	5′CCA TAG ATT CCA TTG GTG CTC GAA CAG TGA C
$T_{d31(5C)}$	5′CCA TAG ATC GCA TTG GTG CTC GAA CAG TGA C
$T_{d31(5G)}$	5′CCA TAG ATG GCA TTG GTG CTC GAA CAG TGA C
$T_{d31(1A)}$	5′CCA TAG ATA GCA ATG GTG CTC GAA CAG TGA C
$T_{d31(1C)}$	5′CCA TAG ATA GCA CTG GTG CTC GAA CAG TGA C
$T_{d31(1G)}$	5′CCA TAG ATA GCA GTG GTG CTC GAA CAG TGA C
$T_{d31(6A)}$	5′CCA TAG AAA GCA GTG GTG CTC GAA CAG TGA C
$T_{d31(6C)}$	5′CCA TAG ACA GCA GTG GTG CTC GAA CAG TGA C
$T_{d31(6G)}$	5′CCA TAG AGA GCA GTG GTG CTC GAA CAG TGA C
T_{d26}	5′CCA TAG ATA GCA TTG GTG CTC GAA CA
P_{d18+5}	5′Cy3 TGT TCG AGC ACC AAT GCT
$T_{d26\ (5C)}$	5′CCA TAG ATC GCA TTG GTG CTC GAA CA
$P_{d18+5\ (5G)}$	5′Cy3 TGT TCG AGC ACC AAT GCG
Surface Plasmon Resonance	
T_{d20}	5′ACA GTC CCT GTT CGG XCG CG
P_{d37}	5′biotin TAG ATC AGT CATGCTCCGCGCCCGAACAGGGACTGTG
Footprinting assays	
T_{d43}	5′Cy3 CCA TAG ATA GCA TTG GTG CTC GAA CAG TGA CAA TCA GTG TAG A
P_{d30}	5′TCT ACA CTG ATT GTC ACT GTT CGA GCA CCA
P_{d30+5}	5′ACT GTT CGA GCA CCA ATG CT

site (P-site; cleavage at −17) (Fig. 1*C*). Therefore, when EFdA-TP inhibits RT as an ICT it acts as a translocation-defective RT inhibitor. In turn, footprinting assays at sites where EFdA acts as a DCT (such as P6) demonstrated that $T/P_{EFdA\text{-}MP}$ is translocated to the P-site (Fig. 1*C*). Collectively, these experiments show that EFdA-TP can act both as an ICT and as a DCT depending on the template sequence and how it allows translocation of RT on $T/P_{EFdA\text{-}MP}$ (Figs. 1, 8, and 9).

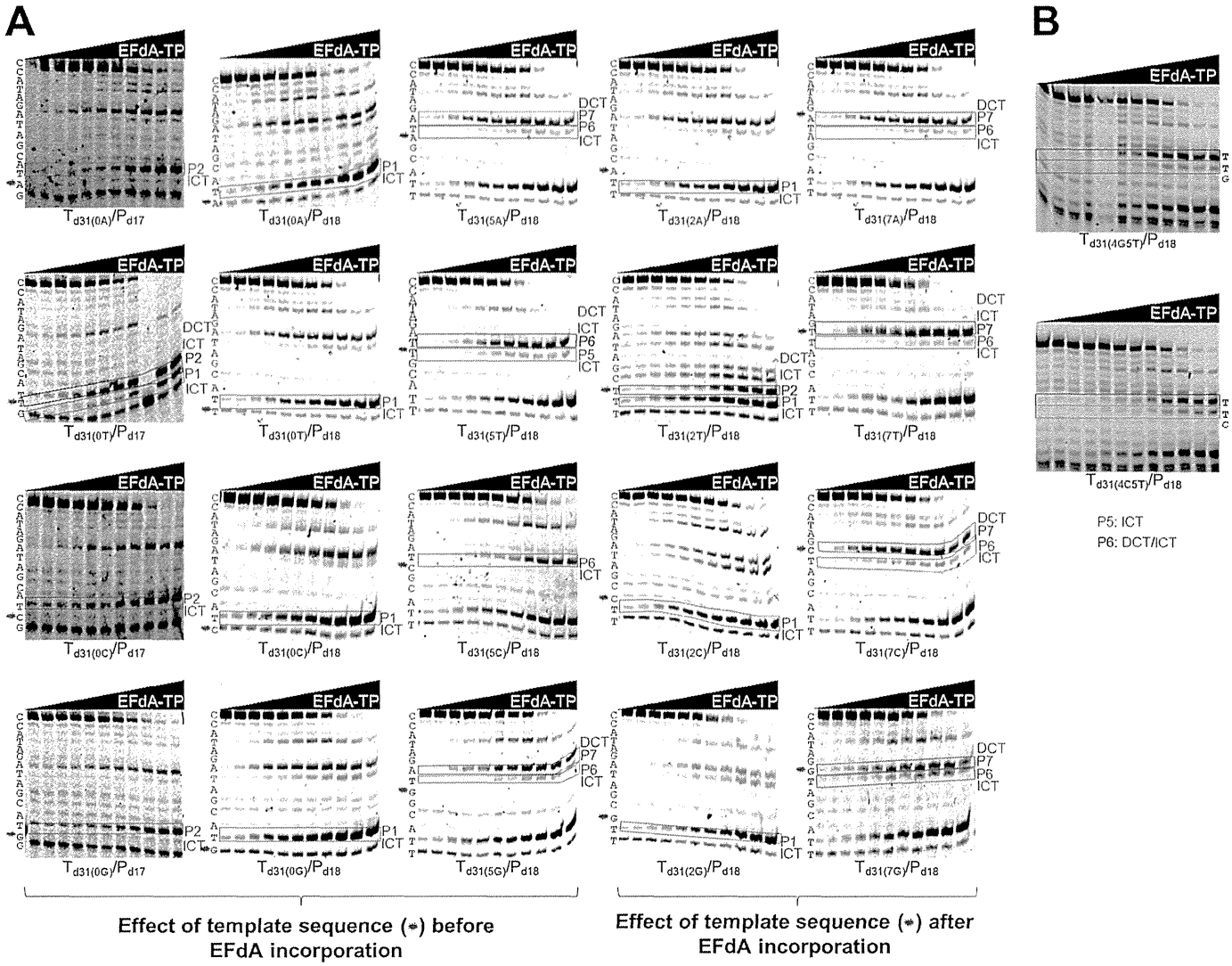

FIGURE 2. **Effect of template sequence on mechanism of inhibition by EFdA-TP.** Primer extension assays were performed by incubating various DNA/DNA T/Ps with 20 nM RT for 15 min in the presence of 10 μM dNTPs, 6 mM $MgCl_2$, and increasing concentrations of EFdA-TP. The sequence of the template is shown next to the gels. Twenty templates with A, T, C, or G at the P0, P2, P5, and P7 positions were used. The nucleotides that vary are shown in *blue* color and indicated with an *asterisk* next to the gel bands. In *red* color, we highlight the T positions where EFdA-TP is expected to be incorporated. Immediate and delayed chain terminations are shown in *red* and *green boxes*, respectively. *Blue* color and *asterisks* highlight the positions of the nucleotides that vary among different gels.

The Mechanism of RT Inhibition by EFdA-TP Is Sequence-dependent—To further explore the effect of the T/P sequence on the EFdA-TP inhibition mechanism, we used a series of oligonucleotides that vary at positions upstream or downstream from the sites of EFdA-MP incorporation (Table 1). As a control we used ddATP, which always acts as a canonical ICT (data not shown).

With regard to the effect of changes before the site of EFdA-MP incorporation, remarkably we found that a single change in the template sequence can change the inhibition mechanism: the presence of C at a template position prior to the P6 site leads to exclusive ICT (Fig. 2*A*, $T_{d31(5C)}/P_{d18}$). In contrast, the presence of A, G, or T at the same template position leads primarily to DCT (Fig. 2*A* and Table 2; $T_{d31(5A)}/P_{d18}$, $T_{d31(5G)}/P_{d18}$, and $T_{d31(5T)}/P_{d18}$), although the presence of bands at the sites of EFdA incorporation (P6, P6, and P5, respectively) suggested an additional but less pronounced ICT mode of inhibition as well (none of these stopping patterns were observed in the absence of EFdA-TP).

Introducing a C before the incorporation site of EFdA-MP does not appear to always result in strong ICT. When we changed the P4 site of $T_{d31(4G5T)}/P_{d18}$ to a C ($T_{d31(4C5T)}/P_{d18}$), we still observed a primarily DCT mode of inhibition (Fig. 2*B*), suggesting that sequences before and after the EFdA-MP incorporation site contribute to the preferred mechanism of inhibition.

EFdA-TP acted as an ICT at the P1 site regardless of the type of preceding nucleotide (Fig. 2*A*, gels in *second column*). To determine whether this strong preference is due to the upstream (P0) position being provided to the enzyme already in double-stranded DNA form (last primer nucleotide), we repeated the experiments using a shorter primer that stopped one position before the EFdA-MP incorporation site. The data shown in Fig. 2*A*, *column 1*, show that there was still ICT inhibition in all cases, whereas only in the case of $T_{d31(0T)}/P_{d17}$ was there an apparent mixture of ICT and DCT.

We also tested the effect of template sequence at one position after the P6 or P1 site of EFdA-MP incorporation (P7 and P2

sites in Fig. 2*A*, *columns 4* and *3*, respectively). We generally found no significant changes in the type of inhibition mechanism with the exception of $T_{d31(2T)}/P_{d18}$, which was now inhibited by both ICT and DCT instead of only ICT. Collectively, these results indicate that the mechanism of inhibition by EFdA can be influenced by the template sequence before and after the site of incorporation.

TABLE 2

Effect of template sequence on mechanism of action of EFdA-TP

The mechanism of inhibition by EFdA-TP was determined by the results in Fig. 2. Changes in the template sequences are indicated in bold.

T/P	Mechanism of action
Effect of template sequence *before* EFdA-MP incorporation	
$T_{d31(0A)}/P_{d17}$	P2: ICT
$T_{d31(0T)}/P_{d17}$	P1: ICT; P2: DCT/ICT
$T_{d31(0C)}/P_{d17}$	P2: ICT
$T_{d31(0G)}/P_{d17}$	P2: ICT
$T_{d31(0A)}/P_{d18}$	P1: ICT
$T_{d31(0T)}/P_{d18}$	P1: ICT
$T_{d31(0C)}/P_{d18}$	P1: ICT
$T_{d31(0G)}/P_{d18}$	P1: ICT
$T_{d31(5A)}/P_{d18}$	P6: ICT; P7: DCT
$T_{d31(5T)}/P_{d18}$	P5: ICT; P6: DCT/ICT
$T_{d31(4C5T)}/P_{d18}$	P5: ICT; P6: DCT/ICT
$T_{d31(5C)}/P_{d18}$	P6: ICT
$T_{d31(5G)}/P_{d18}$	P6: ICT; P7: DCT
Effect of template sequence *after* EFdA-MP incorporation	
$T_{d31(2A)}/P_{d18}$	P1: ICT
$T_{d31(2T)}/P_{d18}$	P1: ICT; P2: DCT/ICT
$T_{d31(2C)}/P_{d18}$	P1: ICT
$T_{d31(2G)}/P_{d18}$	P1: ICT
$T_{d31(7A)}/P_{d18}$	P6: ICT; P7: DCT
$T_{d31(7T)}/P_{d18}$	P6: ICT; P7: DCT/ICT
$T_{d31(7C)}/P_{d18}$	P6: ICT; P7: DCT
$T_{d31(7G)}/P_{d18}$	P6: ICT; P7: DCT

EFdA-TP Binds RT Tighter than the Natural Substrate dATP—Because EFdA-TP inhibits RT very efficiently, we wanted to examine and compare the binding affinity of the inhibitor and dATP with the enzyme. Therefore, we used SPR to determine the dissociation constant K_d for EFdA-TP and dATP. A two-state reaction protocol that assumes a 1:1 binding of substrate (EFdA-TP or dATP) to an immobilized ligand (RT) followed by a conformational change ("closing" of fingers subdomain) to form a stable complex (32–36) was used to analyze the SPR data. It is also assumed that a substrate in a complex that has undergone a conformational change can only dissociate if the conformational change is first reversed. This analysis generated the following kinetic values: k_{a1}, the association rate constant for substrate binding; k_{d1}, the dissociation rate constant for substrate from the complex; k_{a2}, the forward rate constant for the conformational change; k_{d2}, the reverse rate constant for the conformational change; and K_d, the overall equilibrium dissociation constant, which for this type of two-state reaction protocol is defined by $(k_{d1}/k_{a1})\cdot(k_{d2}/(k_{d2} + k_{a2}))$. Fig. 3 shows that, using the T_{d20}/P_{d37}, the K_d for dATP is about 10 times higher than that of EFdA-TP. Hence, RT can bind EFdA-TP considerably more tightly than the natural substrate. This difference in the K_d of dATP and EFdA-TP is mostly due to an increased association rate for substrate binding (k_{a1}) and increased forward rate constant for the conformational change (k_{a2}) in the case of EFdA-TP (Fig. 3).

RT Incorporates EFdA-TP Very Efficiently by Stalling Full Extension of the Terminated Primer—To further understand the biochemical basis of the strong RT inhibition by EFdA-TP, we compared the incorporation efficiency of EFdA-TP with that of the natural substrate dATP under pre-steady state con-

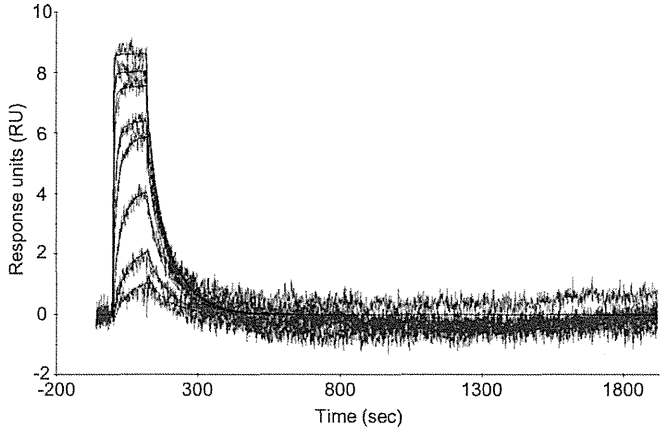

Nucleotide	$K_{d,dNTP}$ / nM	k_{a1} / $M^{-1}s^{-1}$	k_{d1} / s^{-1}	k_{a2} / s^{-1}	k_{d2} / s^{-1}
EFdA-TP	18.6 (1)	$94.7\cdot10^4$ (1)	0.026 (1)	0.010 (1)	0.0224 (1)
dATP	192.8 (10.4)	$3.8\cdot10^4$ (0.04)	0.020 (0.8)	0.001 (0.1)	0.0006 (0.03)

FIGURE 3. **SPR to determine the kinetic constants of EFdA-TP and dATP binding to HIV-1 RT.** Nucleotide binding was performed by using RT covalently cross-linked to T_{d37}/P_{d20}, which has a 5′-biotinylated DNA template and a ddGMP incorporated at the primer. The RT-DNA_{ddGMP} complex was immobilized on a streptavidin sensor chip, and increasing concentrations of dATP or EFdA-TP were flowed to allow nucleotide association and dissociation. A two-state reaction protocol was used to analyze the SPR data, which assume a 1:1 binding of substrate (EFdA-TP or dATP) to an immobilized ligand (RT) followed by a conformational change (closing of fingers subdomain) to form a stable complex. The graph shows the association and dissociation of EFdA-TP over time. This analysis generated the following kinetic values: k_{a1}, the association rate constant for substrate binding; k_{d1}, the dissociation rate constant for substrate from the complex; k_{a2}, the forward rate constant for the conformational change; k_{d2}, the reverse rate constant for the conformational change; and K_d, the overall equilibrium dissociation constant, which for this type of two-state reaction protocol is defined by $K_d = (k_{d1}/k_{a1})\cdot(k_{d2}/(k_{d2} + k_{a2}))$. The -fold change of the various constants is shown in *parentheses*.

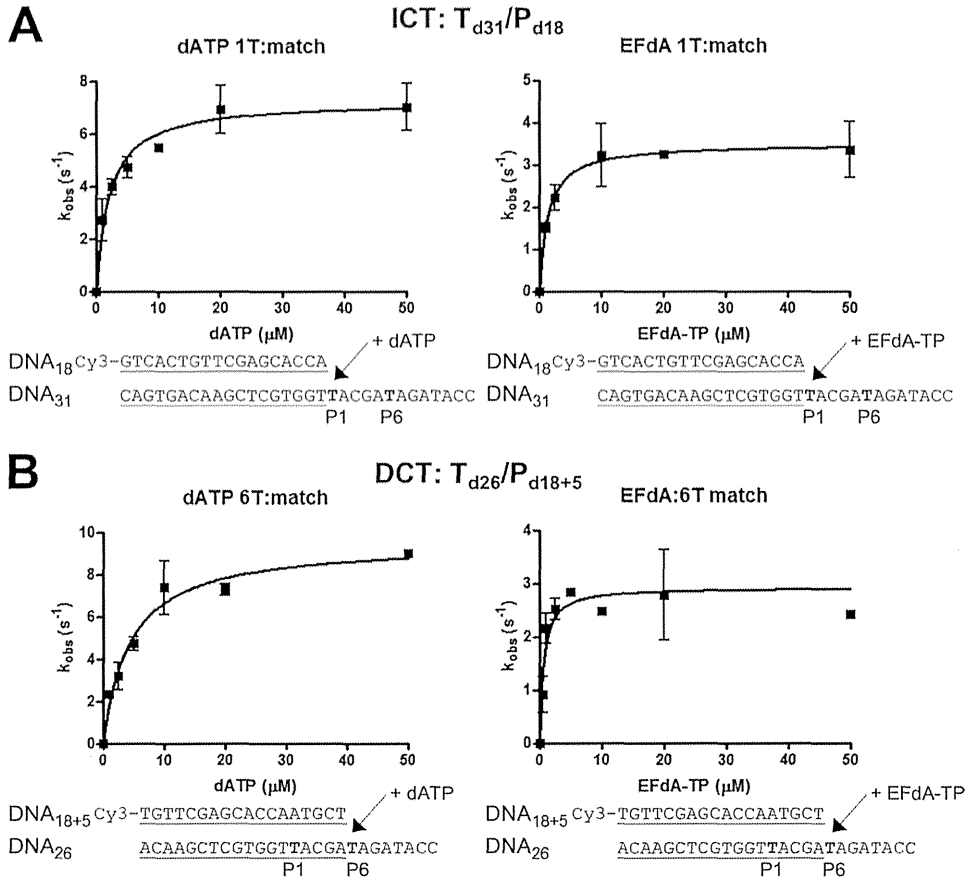

C

T/P	match	k_{pol} (s^{-1})	$K_{d\text{-dNTP}}$ (μM)	$k_{pol}/K_{d\text{-dNTP}}$ (μM^{-1} s^{-1})	Selectivity
T_{d31}/P_{d18} ICT	dATP:1T	7.2 ± 0.3	2.1 ± 0.4	3.4	1
	EFdA-TP:1T	3.4 ± 0.7	1.2 ± 0.2	2.8	0.8
T_{d26}/P_{d18+5} DCT	dATP:6T	9.8 ± 0.4	5.1 ± 1.8	1.9	1
	EFdA-TP:6T	3.1 ± 0.4	0.7 ± 0.2	4.4	2.3

Values are determined from three independent experiments. Positions where EFdA-TP acts as an ICT or DCT are shown in red and green, respectively.

FIGURE 4. **Pre-steady state kinetics of correct single nucleotide incorporation of EFdA-TP and dATP by HIV-1 RT.** Preincubated HIV-1 RT (50 nM) and T_{d31}/P_{d18} (*A*) or T_{d26}/P_{d18+5} (50 nM) (*B*) were mixed by a quench-flow instrument with various concentrations of EFdA-TP or dATP for reaction times varying between 5 ms and 2 s. The amount of product at different reaction times was fit to the burst equation (Equation 1) to obtain burst phase rates of nucleotide incorporation. Observed rate constants were then plotted using a hyperbolic equation (Equation 3) to estimate k_{pol} and $K_{d(dNTP)}$ (*A* and *B*). The sequences of the T/Ps are shown below the plots, and the calculated constants are shown in *C*. *Error bars* represent S.D. of at least two independent experiments.

ditions. Our results show that RT uses EFdA-TP very efficiently (Fig. 4). Interestingly, we demonstrated that depending on the sequence of the template the selectivity for EFdA-TP over the natural dATP substrate ranges from 0.8- to 2.3-fold. Another independent study using a different T/P showed that the incorporation efficiency of EFdA-TP is 2-fold higher than that of dATP (37). The high incorporation efficiency of EFdA-TP is mostly the result of the higher binding affinity of EFdA-TP (lower dissociation constant K_d). These results are consistent with the SPR data that also showed an increased RT binding affinity for EFdA-TP compared with dATP using another T/P sequence.

Because EFdA-TP differs from the conventional chain terminators and possesses a 3′-OH group, we examined the possibility that there can be additional DNA polymerization events at the EFdA-MP end of $T/P_{EFdA\text{-}MP}$. Primer extension experiments showed that when EFdA-TP acts as an ICT there is eventually slow full extension of the EFdA-MP-terminated primers (Fig. 5*A*). When EFdA-TP acts as a DCT, there is extension of the EFdA-MP primers by only one nucleotide under these conditions (Fig. 5*B*) and very little full extension over the course of hours (not shown). The extension of EFdA-MP-terminated primers has also been reported by Muftuoglu *et al.* (37) in the context of a different sequence and in the presence of higher dNTP and RT concentrations and is consistent with our findings reported here.

We used pre-steady state kinetics to quantify and compare the efficiencies of dNTP incorporation in EFdA-MP-termi-

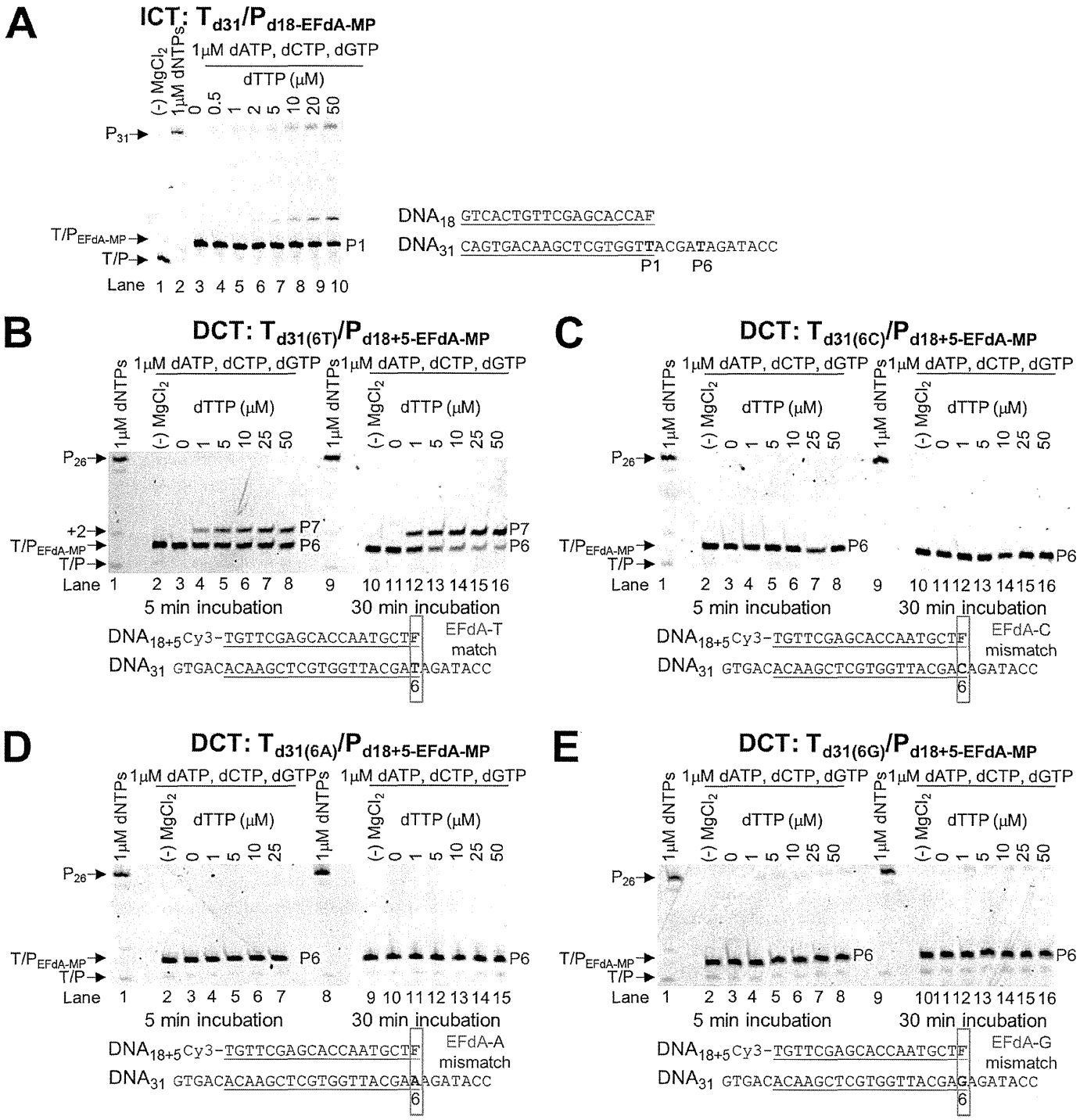

FIGURE 5. **Incorporation of dNTPs into T/$P_{EFdA-MP}$ by HIV-1 RT.** *A*, $T_{d31}/P_{d18\text{-}EFdA\text{-}MP}$ (5 nM) was incubated with 20 nM HIV-1 RT, 6 mM $MgCl_2$, 1 μM dATP, dCTP, dGTP, and increasing concentrations of the next correct dNTP (dTTP, 0–50 μM). The reactions were terminated after 15 min. *B*, $T_{d31}/P_{d18+5\text{-}EFdA\text{-}MP}$ (5 nM) was incubated with 20 nM HIV-1 RT, 6 mM $MgCl_2$, 1 μM dATP, dCTP, dGTP, and increasing concentrations of the next correct dNTP (dTTP, 0–50 μM). The reactions were terminated after 5 and 30 min. *C–E*, various $T_{d31}/P_{d18+5\text{-}EFdA\text{-}MP}$ (5 nM) where EFdA-MP is incorporated as a mismatch were incubated with 20 nM HIV-1 RT, 6 mM $MgCl_2$, 1 μM dATP, dCTP, dGTP, and increasing concentrations of the next correct dNTP (dTTP, 0–50 μM). The reactions were terminated after 5 and 30 min. The sequences of the T/Ps are shown below the gels, and the lanes are numbered for clarity.

nated primers at ICT ($T_{d31}/P_{d18\text{-}EFdA\text{-}MP}$) *versus* DCT ($T_{d26}/P_{d18+5\text{-}EFdA\text{-}MP}$) sites. Consistent with the gel-based results of Fig. 5, *A* and *B*, there was indeed a >400-fold difference in the extension efficiency of the EFdA-MP-terminated primers when different T/Ps were used (Table 3). Interestingly, when we simply changed a single template base from A to C at one position before the EFdA-MP incorporation site (Table 3), we observed that the kinetics of dNTP incorporation on EFdA-MP-terminated primers were dramatically changed, showing a shift from a DCT to ICT mechanism. Using a single different T/P sequence, Muftuoglu *et al.* (37) recently showed that RT can incorporate dCTP after EFdA-MP 400 times more efficiently than it does after AMP (~1.5 *versus* 0.0034 $\mu M^{-1} \cdot s^{-1}$) (38).

TABLE 3

Pre-steady state kinetic parameters of dTTP incorporation on T/P$_{EFdA-MP}$ by HIV-1 RT

Values were determined from three independent experiments. Positions where EFdA-TP acts as an ICT or DCT are shown in red and green, respectively.

T/P	k_{pol} (s^{-1} x 10^{-3})	$K_{d.dTTP}$ (μM)	$k_{pol}/K_{d\text{-}dTTP}$ (μM^{-1} s^{-1} x 10^{-3})	Fold difference
$T_{d31}/P_{d18\text{-}EFdA\text{-}MP}$ ICT	1.8 ± 0.2	38.0 ± 7.3	0.05	1
$T_{d26}/P_{d18+5\text{-}EFdA\text{-}MP}$ DCT (Template 5A)	7.6 ± 1.6	0.35 ± 0.1	22	440
$T_{d26\,(5C)}/P_{d18+P5\,(5G)\text{-}EFdA\text{-}MP}$ ICT (Template 5C)	4.6 ± 0.1	9.45 ± 3.2	0.5	10

TABLE 4

Pre-steady state kinetic parameters of EFdA-TP and dATP match and mismatch incorporation by HIV-1 RT

Values were determined from three independent experiments. Positions where EFdA-TP acts as an ICT or DCT are shown in red and green, respectively. The different templates vary in position X: G, C, or A.

T/P	match/mismatch	k_{pol} (s^{-1} x 10^{-3})	$K_{d.dNTP}$ (μM)	$k_{pol}/K_{d\text{-}dNTP}$ (μM^{-1} s^{-1} x 10^{-3})
$T_{d31(1X)}/P_{d18}$ ICT	EFdA-TP:1T	3,400 ± 700	1.2 ± 0.2	2,833
	EFdA-TP:1G	2.3 ± 0.1	0.8 ± 0.2	2.9
	EFdA-TP:1C	8.6 ± 1.6	8.5 ± 1.2	1.0
	EFdA-TP:1A	3.0 ± 0.5	1.5 ± 0.4	2.0
	dATP:1T	7,200 ± 300	2.1 ± 0.4	3,429
	dATP:1G	18.3 ± 2.0	28.0 ± 4.5	0.7
	dATP:1C	2.4 ± 0.5	1.8 ± 0.1	1.3
	dATP:1A	1.8 ± 1.3	66.0 ± 17.8	0.03
$T_{d31(6X)}/P_{d18+5}$ DCT	EFdA-TP:6T	3,100 ± 400	0.7 ± 0.2	4,429
	EFdA-TP:6G	23.8 ± 4.0	9.2 ± 2.4	2.6
	EFdA-TP:6C	24.4 ± 1.9	17.2 ± 0.1	1.4
	EFdA-TP:6A	8.4 ± 1.3	9.7 ± 2.6	0.9
	dATP:6T	9,800 ± 400	5.1 ± 1.8	1,922
	dATP:6G	8.8 ± 1.1	2.8 ± 0.6	3.1
	dATP:6C	2.9 ± 0.1	3.6 ± 0.7	0.8
	dATP:6A	1.7 ± 0.5	19.8 ± 1.9	0.1

EFdA-TP Is Efficiently Incorporated as a Mismatch but with No Further Extension—The inhibition and incorporation experiments suggest that EFdA-TP can be used by RT as a substrate for DNA polymerization at levels even better than the natural dATP substrate. Using pre-steady state kinetics, we extended this finding by showing that EFdA-TP can be incorporated very efficiently not only as a cognate substrate but also as a mismatched substrate (Table 4). Specifically, EFdA-TP is incorporated as a mismatch more efficiently against a G than an A or a C. We also found that the template sequence affects the misincorporation efficiency in different ways for EFdA-TP and dATP. Hence, EFdA-MP is misincorporated more efficiently than dAMP at the P1 sites (ICT mechanism) when the mispairing base is opposite G or A, but not C (Table 4). In contrast, the misincorporation efficiencies of EFdA-MP and dAMP are similar at the P6 site (DCT mechanism) opposite G and C, whereas EFdA-MP is misincorporated more efficiently than dAMP opposite A. In addition, we tested the extension of primers terminated with misincorporated EFdA-MP (EFdA-MP opposite a C, A, or G) and found that there is no dNTP addition even at higher dNTP concentrations or incubation times (Fig. 5, *C*, *D*, and *E*) in contrast to the one-nucleotide extension of T/P$_{EFdA-MP}$ with EFdA-MP opposite the cognate base T (Fig. 5*B*).

Delayed Chain Termination Protects EFdA-MP from Excision—One of the major mechanisms of resistance to NRTIs is the ATP-based excision of the chain terminator by RT (39, 40). The product of this excision reaction is a tetraphosphate (NRTI-MP-ATP) and an unblocked primer that RT can use to resume DNA synthesis (41). For excision to occur, the NRTI-MP end of the chain-terminated primer should be positioned at the N-site (42). Our footprinting data in Fig. 1*C* establish that the translocation state, which reflects the position of RT on DNA, can be affected by the nucleic acid sequence. Specifically, in the absence of dNTP, $T_{d43}/P_{d30\text{-}EFdA}$ is bound by RT in a pre-translocation mode (Fig. 1*C*, *lane 7*, *left* gel), whereas $T_{d43}/P_{d30+5\text{-}EFdA}$ is bound in a post-translocation mode (Fig. 1*C*, *lane 7*, *right* gel). Importantly, these differences in binding lead to differences in the mechanism of EFdA inhibition with immediate chain termination at the site where translocation is not favored (P1 site of T_{d31}/P_{d18}) or delayed chain termination at the site where translocation is indeed favored (P6 site of T_{d31}/P_{d18}; Fig. 1, *B* and *C*). Because binding in a pre-translocation mode allows excision to occur (24, 28, 30), we hypothesized that the post-translocation bound $T_{d26}/P_{d18+5\text{-}EFdA\text{-}MP\text{-}dTMP}$ would be protected from excision. To test this hypothesis, we performed ATP- or PP_i-based phosphorolysis experiments to unblock the following EFdA-MP-terminated template primers: (*a*) $T_{d31}/P_{d18\text{-}EFdA\text{-}MP}$, which binds RT in a pre-translocation mode and is the product of ICT, and (*b*) $T_{d26}/P_{d18+5\text{-}EFdA\text{-}MP\text{-}dTMP}$, which binds RT in a post-translocation mode and is the product of DCT with a dTMP incorporated into the EFdA-MP-terminated primer.

We performed the experiments in the presence of either PP_i or ATP. In the latter case, the excision reaction was coupled with the reverse DNA polymerization because dNTPs were also added in the reaction (rescue conditions). When EFdA-TP is inserted opposite P1 it acts as an ICT (as in $T_{d31}/P_{d18\text{-}EFdA\text{-}MP}$ or $T_{d43}/P_{d18\text{-}EFdA\text{-}MP}$), and the nucleic acid is bound in a pre-translocation binding mode (Fig. 1*C*). In that case, there is some PP_i-based excision of EFdA-MP from the 3′-end of the primer (Fig. 6*A*, *left panel*, *lanes 2–8*), although even in this case it does not appear to be a significant problem because there is facile reincorporation of EFdA-TP as we have shown previously (10). In addition, ATP-based rescue experiments showed that when a high concentration of competing dATP is included in the reaction we can detect rescue of the EFdA-MP-terminated primers (Fig. 6*B*, *lanes 4–11*) that are the ICT inhibition product, suggesting that when EFdA-MP is incorporated at an ICT site it is excised even though this phenomenon does not account for high level excision-based resistance as shown by our published virological data (11). In contrast, when EFdA-TP is inserted opposite P6, it acts as a DCT and allows a single incorporation event, which in the case of $T_{d26}/P_{d18+5\text{-}EFdA\text{-}MP\text{-}dTMP}$ is a dTMP incorporation opposite P7. Under these conditions of DCT, there is a compelling suppression of PP_i-based and ATP-based excision as shown in Fig. 6, *right panels* in *A* (*lanes 10–16*) and *B* (*lanes 15–23*). Hence, at sites of DCT, EFdA-MP-terminated primers are protected from excision, providing a strong advantage for EFdA-TP against excision-based resistance. Furthermore, mismatched primers that have EFdA-MP at the 3′-end are protected from excision (Fig. 6*C*, *lanes 8–12*, *14–18*, and *20–24*).

EFdA-TP and TFV-DP Do Not Always Compete for the Same Incorporation Sites—Because both EFdA and tenofovir are adenosine analogs, we wanted to see whether they would com-

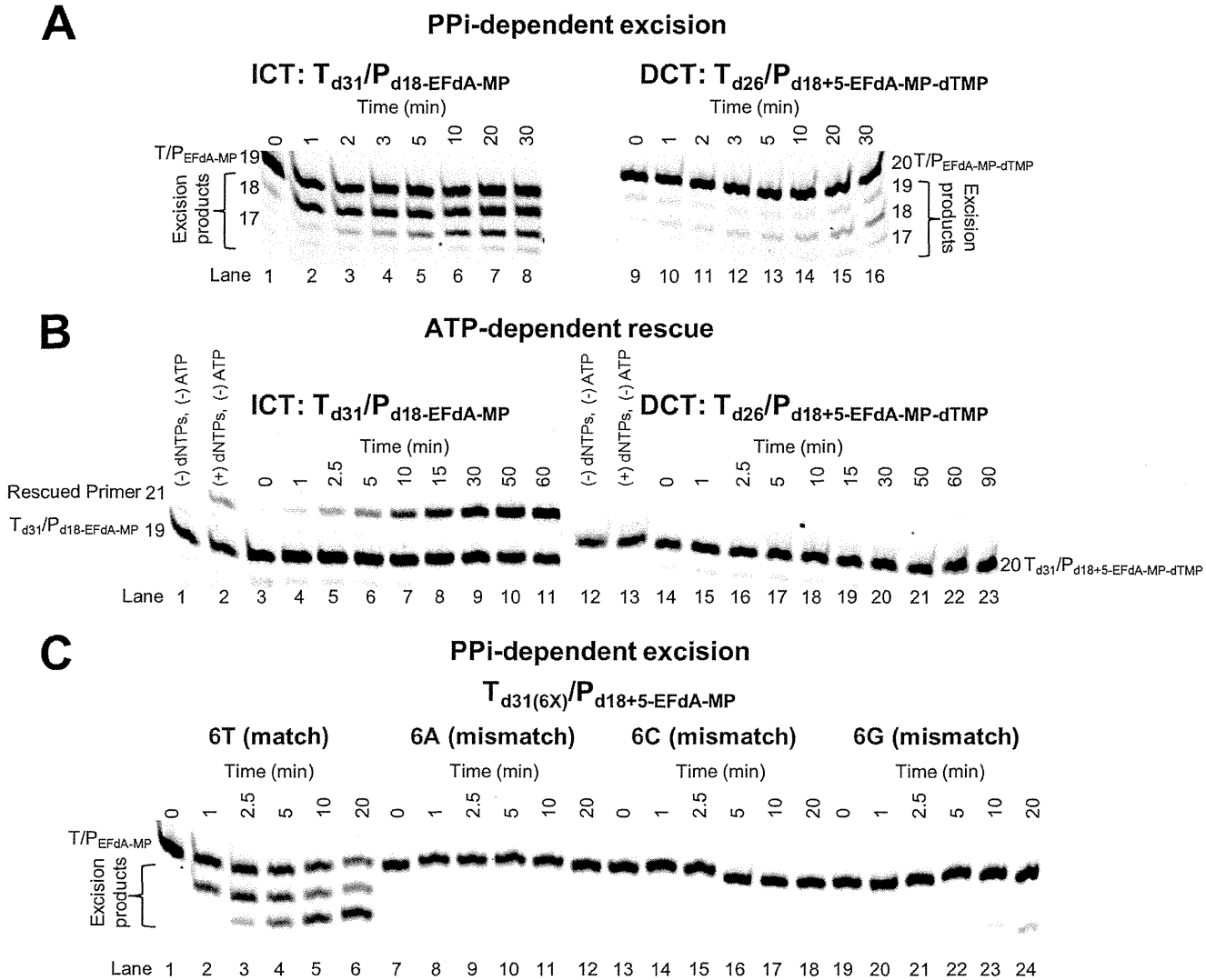

FIGURE 6. **PP_i- and ATP-dependent unblocking of EFdA-MP-terminated primers.** *A*, purified $T_{d31}/P_{d18\text{-}EFdA\text{-}MP}$ or $T_{d26}/P_{d18+5\text{-}EFdA\text{-}MP\text{-}dTMP}$ was incubated with HIV-1 RT in the presence of 6 mM $MgCl_2$ and 150 μM PP_i at 37 °C. Aliquots were removed, and reactions were stopped at the indicated time points (0–30 min). The excision products are shown in *braces*. *B*, purified $T_{d31}/P_{d18\text{-}EFdA\text{-}MP}$ or $T_{d26}/P_{d18+5\text{-}EFdA\text{-}MP\text{-}dTMP}$ was incubated at 37 °C with HIV-1 RT in the presence of 10 mM $MgCl_2$, 3.5 mM ATP, and d(d)NTPs (100 μM dATP, 0.5 μM dTTP, and 10 μM ddGTP for $T_{d31}/P_{d18\text{-}EFdA\text{-}MP}$ or 100 μM dTTP and 10 μM ddCTP for $T_{d26}/P_{d18+5\text{-}EFdA\text{-}MP\text{-}dTMP}$). Aliquots of the reactions were stopped at the indicated time points (0–90 min). *C*, purified $T_{d31(6X)}/P_{d18+5\text{-}EFdA\text{-}MP}$ (where X = T, A, C, or G) was incubated with HIV-1 RT in the presence of 6 mM $MgCl_2$ and 150 μM PP_i at 37 °C. Aliquots were removed, and reactions were stopped at the indicated time points (0–20 min). The excision products are shown in *braces*. The lane *numbers* are shown below each gel.

pete for the same incorporation sites. Surprisingly, when we used the active forms of the two analogs (EFdA-TP and TFV-DP) *in parallel reactions* at concentrations that resulted in approximately the same amount of primer extension (Fig. 7*A*, 2 *versus lane* 3), there were some differences in inhibitor incorporation as judged by stopping patterns. Specifically, although both inhibitors appeared to be incorporated opposite Ts (+6, +8, +10, +17, and +19) (Fig. 7*A*, *lanes* 2 and 3), there was a site that was strongly preferred by EFdA for DCT inhibition (+6 and +7 strong stops with no equivalent stops in the uninhibited *first lane*), whereas there was only moderate inhibition by TFV (weaker stop in the TFV-inhibited *third lane*). Furthermore, the +6 stop was weaker than the +10 stop for TFV but not for EFdA, providing initial evidence that the two adenosine analogs can have different incorporation efficiencies at different sites on the template. To further explore this possibility, we included both TFV-DP and EFdA-TP *in the same reaction* and in varying ratios using a shorter $T_{d31(7C)}/P_{d18}$ that allowed us to better resolve and monitor the EFdA-MP-terminated *versus* the TFV-terminated products. In each of the eight panels of Fig. 7*B*, we used increasing amounts of EFdA-TP in the presence of constant amounts of TFV-DP. Conveniently, we can follow incorporation of EFdA-MP and TFV in the same gels: hence, at the P1 site, the EFdA-MP-terminated primers ($P_{d18\text{-}EFdA\text{-}MP}$) migrate slightly slower than the corresponding TFV-terminated primers ($P_{d18\text{-}TFV}$) (Fig. 7*B*, *red boxes*). At the P6 site, we can compare TFV-based inhibition ($P_{d18+5\text{-}TFV}$) with the EFdA-based inhibition ($P_{d18+5\text{-}EFdA\text{-}MP\text{-}dTMP}$ at P7). We found that EFdA can compete with an excess of TFV more efficiently at the P6 *versus* at the P1 site: for example, in the presence of an excess of TFV (Fig. 7*B*, TFV = 1,000 nM), ~50% of chain termination at P6 is caused by ~31 nM EFdA (Fig. 7*B*, *blue box*), but the same ~50% chain termination at P1 is caused by ~500 nM EFdA (Fig. 7*B*, *red box*). Similar results can be seen at other